Applications

Why Use FLIM

Microscope users often consider the fluorescence lifetime just an additional parameter to separate the signals of different fluorophores. It is certainly correct that different fluorophores usually have different fluorescence lifetimes, and their signals can thus be separated by FLIM. However, reducing the fluorescence lifetime to a mere separation parameter means missing the point of FLIM. FLIM applications are not primarily aiming at separating signals of different fluorophores. Instead, FLIM is used to discriminate *different fractions of the same fluorophore* in different states of interaction with its environment. This is achieved by using a basic property of the fluorescence lifetime: The fluorescence lifetime of a fluorophore depends on its molecular environment but, within reasonable limits, not on its concentration. Molecular effects can thus be investigated independently of the unknown and usually variable fluorophore concentration [53, 60, 75, 226, 299, 338].

Ion concentrations

An excited molecule can dissipate the absorbed energy by interaction with other molecules. The effect is called fluorescence quenching. The fluorescence lifetime, τ, then becomes shorter than the normally observed fluorescence lifetime, τ_0, see Fig. 288, left. One quenching mechanism is 'collisional' quenching, i.e. the collision of the excited molecule with another molecule, atom, or ion. Typical quenchers are oxygen, halogens, heavy metal ions, and a variety of organic molecules. For fluorescence lifetime microscopy it is important that the rate constant of fluorescence quenching depends linearly on the concentration of the quencher. The concentration of the quencher can therefore be directly obtained from the decrease in the fluorescence lifetime. The classic example is quinine, the lifetime of which follows the reciprocal Cl^- concentration over two orders of magnitude. A practical example is shown in Fig. 288, right. A comprehensive overview about quenching by various ions can be found in [226].

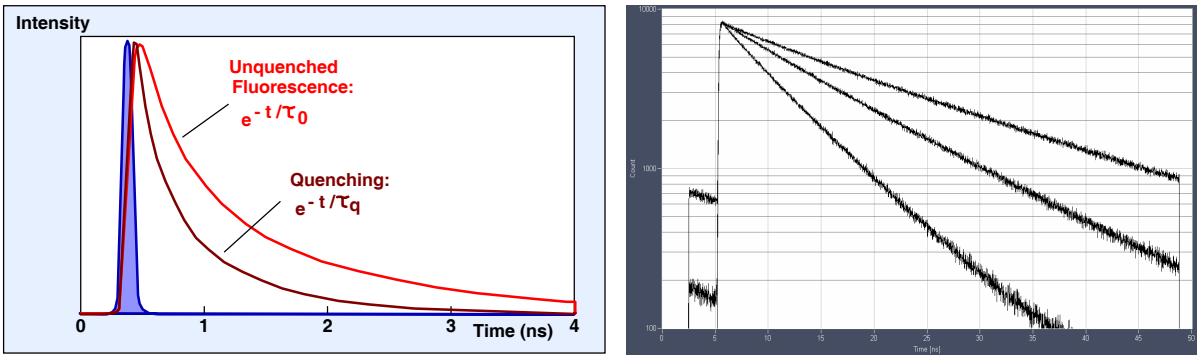

Fig. 288: Left: Fluorescence quenching. Right: Change of the fluorescence lifetime of quinine sulphate with the Cl^- concentration.

Of particular interest to cell biology are Ca^{++} and Cl^-, both of which are important to the function of the neuronal system. Applications of fluorescence-lifetime recording and FLIM to the measurement of Ca^{++} and Cl^- concentrations can be found in [54, 219, 365] and [141, 148, 156, 191], respectively.

Oxygen

Oxygen is an efficient fluorescence quencher for a large number of fluorophores [226], especially those of longer fluorescence lifetime. Strong effects are observed for pyrene, anthra-

cene, and coronene. Unfortunately these compounds absorb and emit in the UV. They are therefore of limited usefulness in microscopy. Strong oxygen quenching is also observed for the phosphorescence of organic ruthenium, europium, platinum and palladium compounds [151, 226, 229, 269, 270]. Unfortunately the phosphorescence lifetimes are so long - from hundreds of nanoseconds to many microseconds - that they are difficult to record in combination with the high laser pulse-repetition rates and fast scan rates used in modern laser scanning microscopes. bh have therefore developed a phosphorescence lifetime imaging techniques based on laser modulation and dual-time-base recording [51], see 'Phosphorescence Lifetime Imaging (PLIM)', page 125.

Oxygen Effect on NADH and FAD fluorescence

Oxygen has a strong effect on the fluorescence of the endogenous fluorophores NADH and FAD. Chance et al. defined a 'redox ratio' that is a direct indicator of the amount of oxygen used in the mitochondria of the cells [93, 94]. Indirectly, oxygen has an influence on the ratio of bound and unbound NADH [154, 101, 103]. Effects of oxygen probably exist also for other endogenous fluorophores [313, 314]. Oxygen-induced changes of the decay profiles of endogenous fluorophores can be expected to become important with the introduction of FLIM into clinical applications.

Binding to Proteins, Protein Configuration

Many fluorescent molecules, including endogenous fluorophores, form complexes with other molecules, in particular proteins. The fluorescence spectra of these different conformations can be virtually identical, but the fluorescence lifetimes are often different. The exact mechanism of the lifetime changes is not always clear. The most likely mechanisms are fluorescence quenching and a change in the configuration of the fluorophore which, in turn, changes the rate of internal non-radiative decay. In practice, for almost all dyes the fluorescence lifetime depends more or less on the binding to proteins, or lipids [202, 226, 300]. When a fluorophore is bound to a protein also the protein configuration may have an influence on the fluorescence lifetime [59]. Fluorescence lifetimes of flavinols in plant cells recorded by TCSPC FLIM were found to be as short as 45 ps, probably due to extremely efficient quenching [260]. Kirchberg et al. [200] found changes in the decay profile of Lucifer Yellow depending on the conformation of the protein to which it was bound. A glucose sensor based on this mechanism has been described in [310]. An effect of target protein configuration has even been found for EGFP which had long believed to be insensitive to its environment [155]. Lifetime changes of diphenylhexatriene (DPH) depending on the cholesterol concentration were used in [167]. Davey et al. found an increase of the fluorescence lifetime of dil-C18 and Alexa-488-labelled IgE in local membrane structures [107]. Garcia et al. used a fluorescently labelled ATP analog to detect actomyosin states in muscle sarcomeres [146]. An application of environment-dependent lifetime variation to the analysis of histological samples has been described in [125]. Environment-dependent changes of fluorescence parameters have even been observed for quantum dots and nano-particles [91, 104, 150, 375]. There is an enormous amount of fluorophores used in microscopy today [173, 338], and only a few of them have been tested for target-specific lifetime changes. The most promising ones are those of medium and low quantum efficiency. These are most likely to be influenced by the local molecular environment. FLIM users are encouraged to keep eyes on lifetime changes that may be suitable as probe functions, see also section 'Near-Infrared FLIM' of this handbook.

Binding to DNA and RNA

It has been shown by van Zandvoort et al. that the fluorescence lifetime of SYTO13 is different when bound to DNA or RNA [355]. The effect has been used to measure the RNA:DNA

ratio in living bacteria cells and bacteria colonies [362]. Douma et al. used the environment-dependent lifetime of SYTO13 and SYTO41 to differentiate between different cells and cell structures in blood vessels [120].

Endogenous Fluorophores, Effect of Metabolic Activity

Most endogenous fluorophores are mixtures of slightly different compounds, with almost identical spectra but different fluorescence lifetimes [314, 315, 316]. The composition of the mixture may vary, and thus induce a change in the amplitudes of the decay components and in the apparent lifetime. Moreover, the lifetimes depend on the binding to proteins, on the oxygen concentration [313], or other metabolic parameters. The most common endogenous fluorophores are NADH and FAD which both exist in a bound and in an unbound form. The lifetime differences between the forms are substantial, and bound and unbound fractions can be easily distinguished by FLIM [224, 272]. Both the fluorescence lifetimes of the decay components and the relative amplitudes have been found sensitive to the metabolic state of cells and tissue [68, 101, 102, 103, 154, 323, 324].

Local Viscosity

Local viscosity can be sensed by 'molecular rotors'. These are fluorophores that have a high degree of internal flexibility. Rotation inside the fluorophore provides for a radiationless decay path. The non-radiative decay rate changes with the viscosity of the solvent. Viscosity measurement by FLIM with a Bodipy-based molecular rotor has been demonstrated in [180, 220, 232,]. In general, the fluorescence lifetime of any fluorophore of high molecular flexibility can be expected to depend on the viscosity of the environment. Lifetime variation of dialkyl-indocarbocyanines due to micro-viscosity changes in cell membranes has been used in [342].

Influence of Local Refractive Index

The radiative decay rate of a fluorophore depends on the local refractive index [332, 336, 337]. The refractive index varies within biological cells and tissue. The lifetime changes induced by these variations can be used to gain structural information about biological specimens and to study membrane effects, e.g. the transition of a bacterium or a virus through a cell membrane [348, 349].

Proximity to metal surfaces, binding to nanoparticles

Extremely strong effects on the decay rates must also be expected if dye molecules are bound to metal surfaces, especially to metallic nano-particles [87, 147, 241, 286, 297]. Proximity to metal surfaces changes both the radiative and non-radiative decay rates. It can happen that the radiative rate increases dramatically. The result is a decrease in the fluorescence lifetime without a decrease (or even with an increase) in intensity, accompanied by an increase in photostability. Similar, yet less dramatic effects have been reported also for non-metallic nanoparticles. They are interesting when such particles are used as carriers of drug delivery. TCSPC measurements on Cy3 encapsulated in calcium phosphate nanoparticles have shown reduced non-radiative and increase radiative decay rates, resulting in a 20 fold increase in brightness [256, 258]. The use of cyanine-loaded lipid nanoparticles was demonstrated in [343], and improved fluorescence efficiency was verified by TCSPC. Changes of the fluorescence lifetime depending on the substrate a protein construct is resting on were exploited in [181].

Solvent Polarity

The molecular conformation of a fluorophore and thus its fluorescence behaviour is also influenced by the solvent properties, especially the solvent polarity [61, 226]. Therefore, the fluorescence lifetimes of many fluorophores depend more or less on the solvent polarity [166].

Moreover, when a molecule enters the excited state the solvent molecules around it re-arrange. Consequently, energy is transferred to the solvent, with the result that the emission spectrum is red-shifted. Solvent (or spectral) relaxation in water happens on the time scale of a few ps. However, the relaxation times in viscous solvents and in dye-protein constructs can be of the same order as the fluorescence lifetime. The effects can be measured by TCSPC [285]; applications of spectral relaxation to cell imaging have not been reported yet.

pH Sensors

Many fluorescent molecules have a protonated and a deprotonated form. The equilibrium between both depends on the pH. If the protonated and deprotonated form have different lifetimes the apparent lifetime is an indicator of the pH. A typical representative of the pH-sensitive dyes is 2',7'-bis-(2-carboxyethyl)-5-(and-6)-carboxyfluorescein (BCECF) [6, 170, 173, 226, 307]. An example is shown in the application part of this chapter. Medintz et al. presented a pH sensor based on a quantum-dot/dopamine conjugate [249]. They determined the mechanism of the lifetime change to be electron transfer within the conjugate.

Ion Concentration

There are fluorescence sensors for various ions. The sensors either undergo collisional quenching by the ions, or perform conformational changes which lead to a change in the fluorescence quantum efficiency. Most of the changes are accompanied by a corresponding change in the fluorescence lifetime. Please see [75, 226, 338] for an overview. The use of Ca^{2+} and Cl^- sensors is described in section 'Measurement of Molecular Environment Parameters', page 194.

Redox Potential

There are fluorophores that change their fluorescence behaviour depending on the redox potential of the local environment. Sensors based on GFP variants are described in [171]. An improved redox sensor based on a modified GFP (roGFPiE) was developed by Avezov et al. Test results obtained in various cells by TCSPC FLIM are described in [10].

Aggregation of Fluorophores

The radiative and non-radiative decay rates depend also on possible aggregation of the dye molecules. The electron systems of the individual molecules in aggregates are strongly coupled. Therefore the fluorescence behaviour of aggregates differs from that of the free molecules. Aggregation is influenced by the local environment; the associated lifetime changes can be used as a probe function. Lifetime heterogeneity due to aggregation was reported for E-Bodipy fluorophores, see [114]. Aggregation has also been used to observe the internalisation of dyes into cells [196]. Lifetime effects may also occur when dye-labelled proteins aggregate. This has been used to observe HIV-1 internalisation into cells [162], and to observe oligomerisation of labelled proteins [172].

Förster Resonance Energy Transfer: FRET

FRET was first theoretically explained by Theodor Förster in 1946 [133, 134]. The effect is also called fluorescence resonance energy transfer or simply resonance energy transfer (RET). Fluorescence resonance energy transfer is an interaction of two molecules in which the emission band of one molecule overlaps the absorption band of the other. In this case the energy from the first molecule, the donor, can transfer into the second one, the acceptor. FRET can result in an extremely efficient quenching of the donor fluorescence and, consequently, in a considerable decrease of the donor lifetime. The energy transfer rate from the donor to the acceptor decreases with the sixth power of the distance. Therefore it is noticeable only at distances shorter than 10 nm [226]. FRET is used as a tool to investigate protein-protein interac-

tion. Different proteins are labelled with the donor and the acceptor, and FRET is used as an indicator of the binding between these proteins. FRET is the most frequent FLIM application. The number of FLIM-based FRET papers has literally exploded in the last couple of years. Please see 'Fluorescence Resonance Energy Transfer (FRET)', page 198.

Electron Transfer

At distances smaller than about 1 nm between an (electron) donor and acceptor photo-induced electron transfer can occur [135, 226]. The excited molecule can either be the electron donor or the electron acceptor. The direction of the electron transfer is determined by the oxidation potential of the donor and the reduction potential of the acceptor. Electron transfer delivers two radicals, both in the ground (S0) state. Both exited singlet states and triplet states can undergo electron transfer at high rates. In solution, the effective transfer rate is usually limited by diffusion. However, in ordered systems (e.g. complexes or adsorbates) the electron transfer rate may become extremely high. Electron transfer is a basic step in photosynthesis. It is also important to the development of organic photovoltaic devices and artificial photosynthesis systems [328]. In biological imaging photo-induced electron transfer, and the radicals produced by it, are a source of photobleaching and photodamage. Electron transfer is a possible explanation of the fact that some fluorophores are highly photostable in solution, but rapidly photobleach when attached to proteins. It also explains why unstained cells survive high exposure to light, while the same cells stained with exogenous fluorophores may not. Although electron transfer may be the basic mechanism of a number of quenching effects it is not explicitly used as a probing function.

Second-Harmonic Generation

Second-harmonic generation (SHG) is an ultra-fast nonlinear process that converts two photons of the incident light into one emitted photon. The wavelength of the emitted photon is exactly one half of the wavelength of the excitation photons. Second-Harmonic generation has nothing to do with fluorescence but often shows up as an ultrafast component in decay curves measured in multiphoton microscopes. Second harmonic components in FLIM data give additional information about the constitution of the tissue under investigation [244]. SHG emission requires some global organisation of the molecules. In biological system it mainly comes from connective tissue, especially from collagen in animal tissue and from cellulose and starch in plant tissue. The ratio of SHG and autofluorescence intensity in mammalian skin is an indicator of skin ageing [204]. SHG may also become important to localise nanoparticles in human skin.

Measurement of Molecular Environment Parameters

pH Imaging

Microscopic pH imaging can be achieved by staining the sample with a pH-sensitive fluorescent probe. These probes usually have a protonated and a deprotonated form. There is an equilibrium between both forms that depends on the pH of the local environment. If both forms have different fluorescence lifetimes the average lifetime is a direct indicator of the pH [226]. A typical representative of the pH-sensitive dyes is 2',7'-bis-(2-carboxyethyl)-5-(and-6)-carboxyfluorescein (BCECF) [173]. In aqueous solution the lifetimes of the protonated form and the deprotonated form have been found 2.75 ns and 3.90 ns, respectively [170]. In the pH range from 4.5 to 8.5 both forms exist, and the fluorescence decay function is a mixture of both decay components. Thus, the lifetime of a single-exponential fit can be used as an indicator of the pH. An example of pH imaging of skin tissue is shown in Fig. 289. A single-exponential lifetime image is shown left, decay curves from different areas of the image are shown right. In areas of low pH fluorescence components of both protonated and deprotonated BCECF are found. The decay profile is therefore double-exponential. In areas of high pH essentially deprotonated BCECF is found, and the decay profile is single-exponential. It should be noted that the lifetimes of free BCECF differ from the lifetimes of BCECF bound in the tissue. The lifetime-pH relation must therefore be calibrated for bound BCECF.

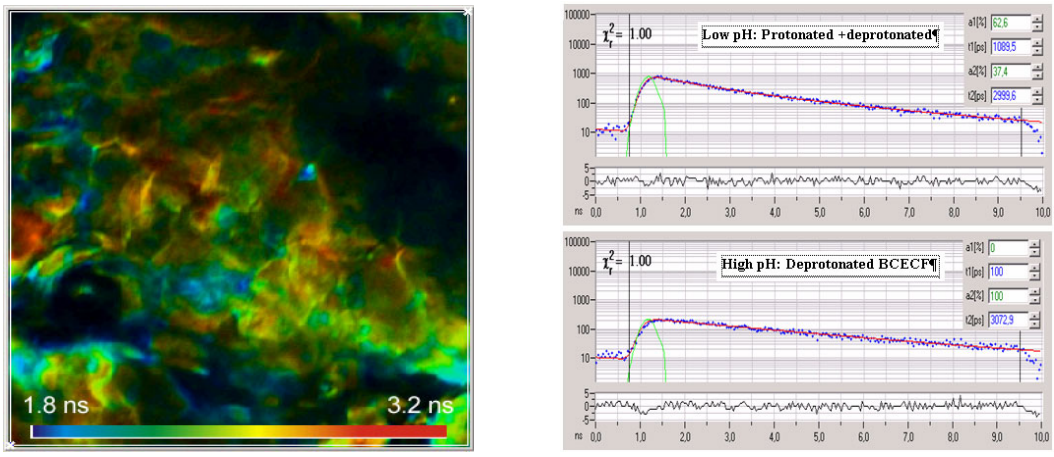

Fig. 289: Left: Lifetime image of skin tissue stained with BCECF. The lifetime is an indicator of the pH. Right: Fluorescence decay curves in an area of low pH (top) and high pH (bottom). LSM 510 NLO with SPC-830 FLIM module, courtesy of Thea Mauro, San Francisco

Calcium Imaging

Ca^{2+} ions are involved in a large number of cell functions, such as intracellular transport, membrane potential, muscle contraction, gene expression, and cell differentiation. There is a wide variety of Ca^{2+} sensors [225, 226, 254]. Most likely, the mechanism of the Ca^{2+}-dependent lifetime change is that the fluorophore has a Ca-bound and a Ca-unbound form of different fluorescence quantum efficiency and thus different fluorescence lifetime. The fluorescence lifetime of the bound form is higher than that of the unbound form. Consequently, the net fluorescence lifetime depends on the Ca^{2+} concentration. It can, however, happen that the fluorescence quantum efficiency of the unbound form is so low that the corresponding lifetime component is no longer observed. In that case, an intensity change but no lifetime change is observed [226]. This is the case for the Fluo sensors, as has been shown for Fluo-4

[54, 137]. However, the traditional Ca^{2+} dyes, such as calcium green and Oregon green, display large lifetime changes and work beautifully for lifetime-based Ca2+ measurement. An examples is shown is Fig. 290.

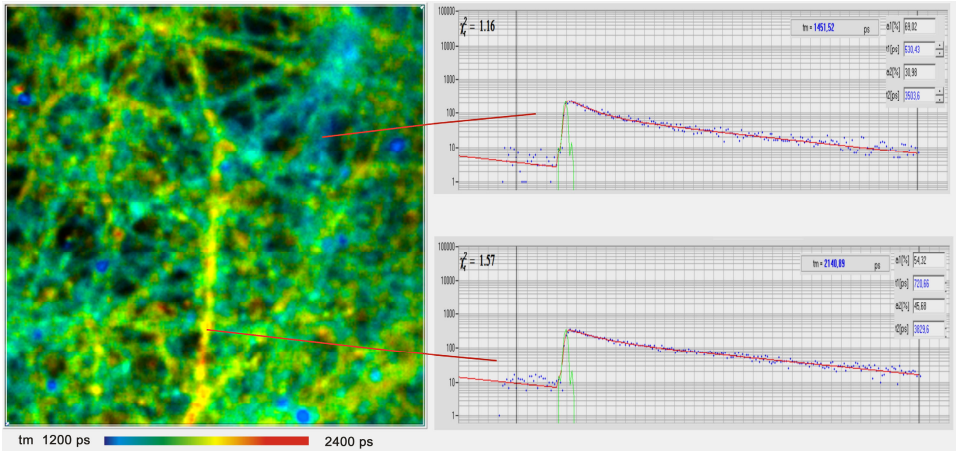

Fig. 290: FLIM image of cultured neurons stained with Oregon green OGB-1 AM. Colour range from τm = 1200 ps (blue) to 2400 ps (red). Decay curves of regions with low Ca (top) and high Ca (bottom) shown on the right. Data courtesy of Inna Slutsky and Samuel Frere, Tel Aviv University, Sackler School of Medicine.

The advantage of FLIM over intensity-based Ca^{2+} imaging is that absolute values of the Ca^{2+} concentration are obtained. This has been used to quantify calcium concentrations in astrocytes of live mice with cortical plaques by multiphoton NDD FLIM [219].

Recording Ca^{++} Transients in Live Neurons

The Ca^{2+} concentration in cells can change within remarkably short periods of time. Recording these 'Ca^{2+} transients' requires a time resolution in the range of less than 50 ms. It is thus usually considered impossible to record Ca^{2+} transients by fluorescence lifetime detection. However, Ca^{2+} transients can easily be recorded by temporal Mosaic FLIM (see page 113) or FLITS (see page 132).

The application of FLITS to the recording of Ca^{2+} transients in live neurons on electrical stimulation has been described in [54] and [137]. A typical result is shown in Fig. 291. Hippocamal cultures were prepared from newborn rats and kept under physiological conditions for 12 to 18 days. The cultures were then loaded with OGB-1 AM, see [137] for details. A Zeiss LSM 7 MP multiphoton microscope with a normal Simple-Tau 150 FLIM system was used to run the FLITS experiments. The cells were stimulated periodically at a fraction of the line clock frequency. To run the experiments, an intensity image was taken by the LSM 7 MP, and an appropriate location for the line scan selected. Then the LSM 7 MP was switched into the line scanning mode. The data acquisition in the FLIM system, the scanning in the LSM 7 MP, and the stimulation were started. The stimulation pulses of 1 ms duration were applied to the cell culture in intervals of 3 seconds [137]. Data acquisition was continued over about 300 seconds, i.e. photons from about 100 stimulation periods were accumulated. The result is shown in Fig. 291, left.

To verify that the FLITS experiment did not cause cell damage or photobleaching a FLIM image was recorded after the FLITS experiment. It is shown in Fig. 291, right. It does not show any cell damage or photobleaching effects along the scanned line. It also shows that the Ca^{2+} concentration returned to the resting level, compare bottom of FLITS image on the left.

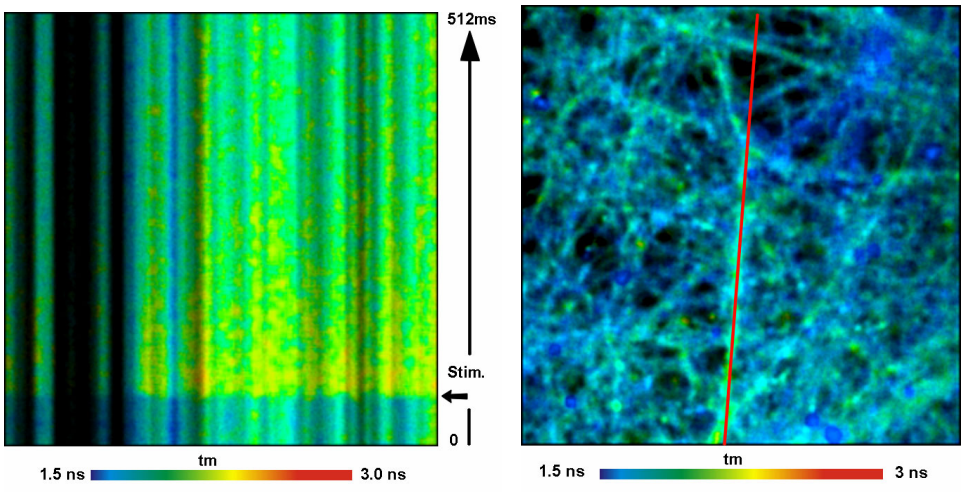

Fig. 291: FLITS of Ca^{2+} transients in live neurons. Left: FLITS image. Right: FLIM image taken after the FLITS recording. Red lines indicates position of FLITS scan. Data courtesy of Inna Slutsky and Samuel Frere, Tel Aviv University, Sackler School of Medicine.

Ca^{2+} recording by temporal mosaic FLIM is shown in Fig. 292. OGB-1 AM was used as a Calcium sensor. The sample was stimulated electrically, and 100 stimulation cycles were accumulated. A Zeiss LSM 7 MP was used for the experiment. With 64 x 64 pixels and a zoom factor of 5, the LSM 7 MP reaches a frame time of 38 ms. 150 milliseconds before every stimulation a recording through the entire 64-element mosaic was started. With the frame time of 38 ms, the acquisition thus runs through the entire mosaic in 2.43 seconds. The result shows clearly the increase in the fluorescence lifetime of the Ca^{2+} sensor in the mosaic elements 4 to 6, and a return to the resting state over the next 10 to 15 mosaic elements (380 to 570 ms).

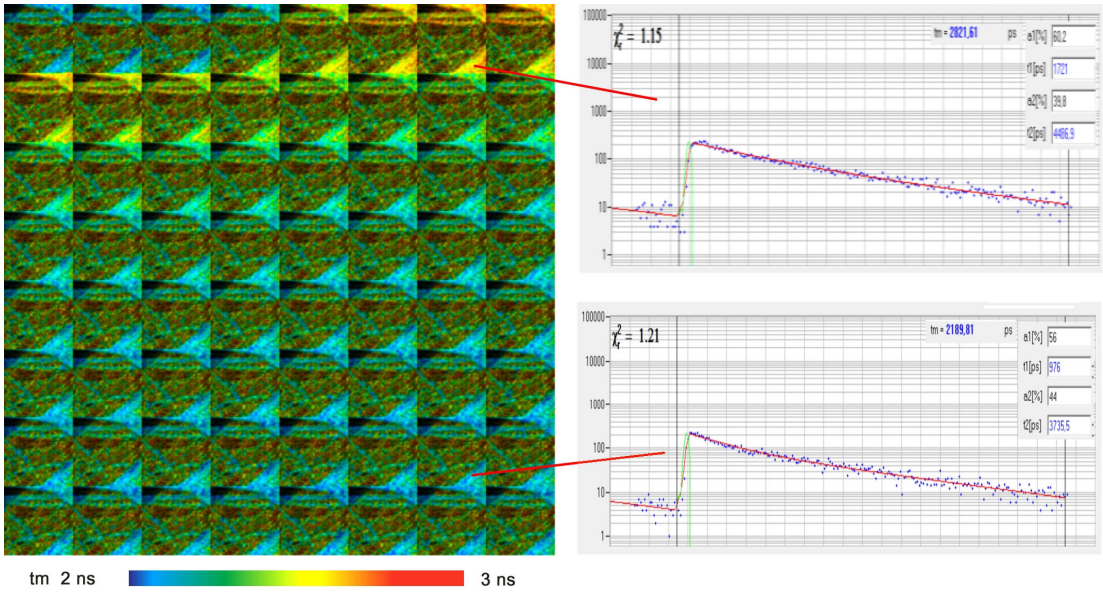

Fig. 292: Temporal mosaic FLIM of the Ca^{2+} transient in cultured neurons after stimulation with an electrical signal. The time per mosaic element is 38 milliseconds, the entire mosaic covers 2.43 seconds. Experiment time runs from upper left to lower right. Photons were accumulated over 100 stimulation periods. Recorded by Zeiss LSM 7 MP and bh SPC-150 TCSPC module. Data courtesy of Inna Slutsky and Samuel Frere, Tel Aviv University, Sackler Faculty of Medicine.

Chloride Imaging

The chloride concentration is important to the function of the neuronal system. An overview on Cl^- imaging is available in [75] and [148]. Measurements of the concentration of intracellular Cl^- in olfactory sensory neurons by TCSPC FLIM were described in [191]. MQAE was used as a fluorescent probe. MQAE is quenched by Cl^-, and the concentration can be calculated from the lifetime change via the Stern-Volmer equation. A bh SPC-730 module was used in conjunction with 2-photon excitation. Because 2-photon excitation does not cause photobleaching and photodamage outside the focal plane the authors were able to obtain z-stacks of the Cl^- concentration in dendrites over depth intervals up to 150 µm. Fig. 293 shows a spinal ganglion of a mouse stained with MQAE. Short lifetimes indicate high Cl- concentration and vice versa.

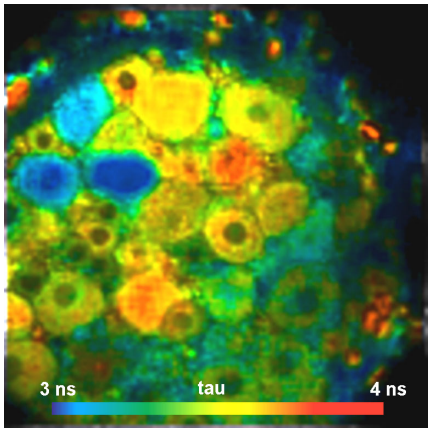

Fig. 293: Spinal ganglion of a mouse stained with MQAE. Short lifetime indicates high Cl- concentration. Data courtesy of Thomas Gensch, Jülich Research Centre, Germany

The same technique was applied to somatosensory neurons in dorsal root ganglia of newborn mice [156]. It could be shown that the somatosensory neurons undergo a transition of Cl^- homeostasis during the first three postnatal weeks. The modulation of chloride homeostasis by inflammatory mediators was investigated in [141]. The influence of the Cl- concentration (and of the pH) on the lifetime of GFP was studied in [8].

Fluorescence Resonance Energy Transfer (FRET)

FRET is an interaction of two fluorophore molecules with the emission band of one dye overlapping the absorption band of the other. In this case the energy from the first dye, the donor, can be transferred to the second one, the acceptor. The energy transfer itself does not involve any light emission and absorption [133, 134, 226]. Förster resonance energy transfer (FRET), or resonance energy transfer (RET), are synonyms of the same effect. The energy transfer rate from the donor to the acceptor decreases with the sixth power of the distance. Therefore it is noticeable only at distances shorter than 10 nm [226]. FRET results in an extremely efficient quenching of the donor fluorescence and, consequently, decrease of the donor lifetime.

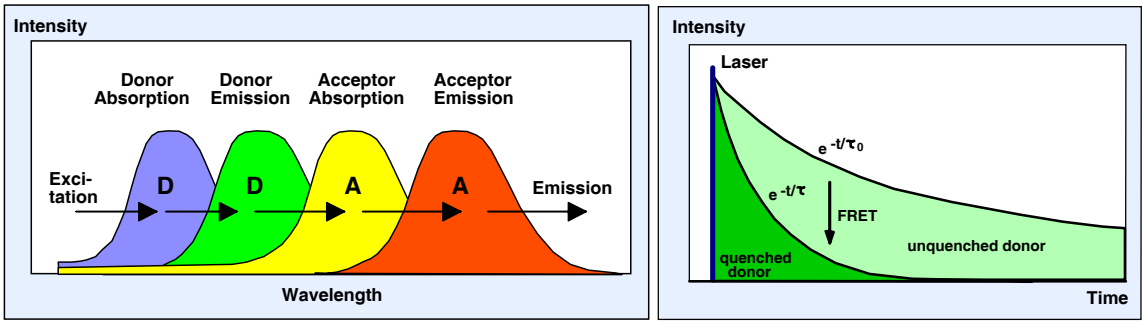

Fig. 294: Fluorescence resonance energy transfer

Because of its dependence on the distance FRET has become an important tool of cell biology [276, 278, 341]. Different proteins are labelled with the donor and the acceptor; FRET is then used to verify whether the proteins are physically linked and to determine distances on the nm scale.

The problem of steady-state FRET techniques is that the concentration of the donor and the acceptor varies throughout the sample. The techniques therefore depend on ratios of the donor and acceptor intensities. However, the FRET-excited acceptor intensity is not directly available. There is 'donor bleedthrough' due to the overlap of the donor fluorescence into the acceptor emission band. Moreover, some of the acceptor molecules are excited directly. Steady-state FRET techniques therefore require careful calibration, including measurements of samples containing only the donor and only the acceptor [158, 177].

The calibration problems can partially be solved by the acceptor photobleaching technique. An image of the donor is taken, then the acceptor is destroyed by photobleaching, and another donor image is taken. The increase of the donor intensity is an indicator of FRET. The drawback is that this technique is destructive, and that it is difficult to use in live cells. In fixed cells, however, the protein structure is changed already by the fixation so that the results are not necessarily correct.

All steady-state techniques have the problem that there is usually a mixture of interacting and non-interacting proteins. Both the fraction of interacting proteins and the distance between the proteins influence the FRET efficiency derived. It therefore cannot be told whether a variation in the FRET efficiency is due to a variation in the distance or a variation in the fraction of interacting proteins.

Single-Exponential FLIM FRET

The use of FLIM for FRET has the obvious benefit that the FRET intensity is obtained from a single lifetime image of the donor [11, 38, 42, 97, 122, 280, 303]. Donor bleedthrough and

directly excited acceptor fluorescence therefore have no influence of FLIM-FRET measurements. The only reference value needed is the donor lifetime in absence of the acceptor. It will be shown later that even this reference lifetime can be obtained from the FLIM-FRET data themselves.

Fig. 295 shows a single-exponential lifetime image of a cultured HEK (human embryonic kidney) cell expressing two interacting proteins labelled with CFP and YFP. The excitation wavelength was 405nm. The fluorescence was recorded through a 480±20 nm filter. It can clearly be seen that the CFP lifetime is reduced in the membrane of the cell and in the Golgy apparatus.

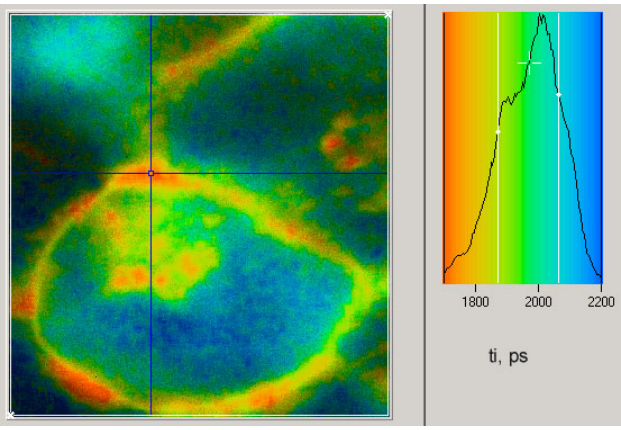

Fig. 295: HEK cell expressing two interacting proteins labelled with CFP (donor) and YFP (acceptor). Single-exponential lifetime image of the donor fluorescence, blue to red corresponds to a lifetime range of 1.7 to 2.2 ns. A lifetime distribution over the pixels is shown on the right. Cells courtesy of Burkhard Wiesner, Leibniz Institute of Molecular Pharmacology (FMP), Berlin, Germany

Single-exponential lifetime images as the one shown in Fig. 295 are very useful to locate the areas in a cell where the labelled proteins interact. It has been shown that for a given efficiency of the optical system and detector and a given excitation power FLIM-based FRET measurements give better accuracy than steady-state techniques [274]. Single-exponential decay measurements do, however, not solve the general problem of the FRET techniques that the total decrease of the donor fluorescence intensity or fluorescence lifetime depends both on the distance of donor and acceptor and the fraction of interacting donor molecules. In the simplest case, a fraction of the donor molecules may not be linked to their targets, or not all of the acceptor targets may be labelled with an acceptor. This can happen especially in specimens with conventional antibody labelling [223]. But even if the labelling is complete by far not all of the labelled proteins in a cell are interacting, and the fraction of interacting protein pairs varies throughout the cell.

Double-exponential FLIM FRET

TCSPC FLIM solves the problem of interacting and non-interacting donor by double-exponential lifetime analysis. The resulting donor decay functions can be approximated by a double exponential model, with a slow lifetime component from the non-interacting (unquenched) and a fast component from the interacting (quenched) donor molecules. If the labelling is complete, as it can be expected if the cell is expressing fusion proteins of the GFP variants, the decay components directly represent the fractions of interacting and non-interacting donor molecules. The composition of the donor decay function is illustrated in Fig. 296.

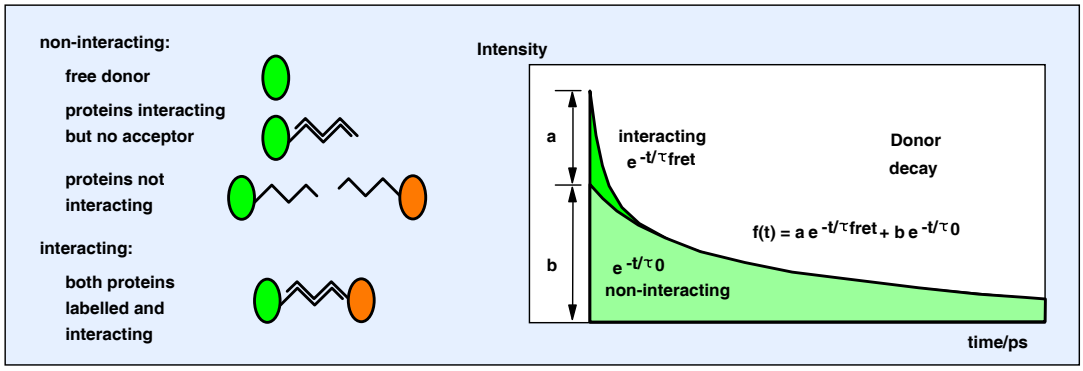

Fig. 296: Fluorescence decay components in FRET systems

Double exponential decay analysis delivers the lifetimes, τ_0 and τ_{fret}, and the intensity factors (amplitudes), a and b, of the two decay components. From these parameters can be derived the true FRET efficiency, E_{fret} , the ratio of the distance and the Förster radius, r/r_0 , and the ratio of the number of interacting and non-interacting donor molecules, N_{fret} / N_0 :

$$E_{fret} = 1 - \tau_{fret} / \tau_0$$

$$(r / r_0)^6 = \tau_{fret} / (\tau_0 - \tau_{fret}) \quad \text{or} \quad (r / r_0)^6 = \frac{1}{E_{fret}} - 1$$

$$N_{fret} / N_0 = a / b$$

Fig. 297 shows the fluorescence decay curves in a selected spot (array of 4 adjacent pixels, selected by the blue crosshair) of Fig. 295.

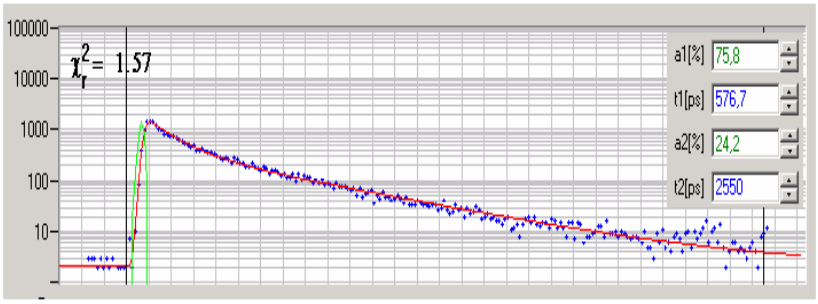

Fig. 297: Fluorescence decay curve in a selected spot of Fig. 295. The decay profile is clearly double-exponential.

The fluorescence decay is indeed double-exponential, with a fast lifetime component, τ_{fret}, of 590 ps, and a slow lifetime component, τ_0, of 2.41 ns.

Fig. 298 shows the result of a double-exponential analysis of the data. The left image shows the ratio of the lifetimes of the non-interacting and interacting donor fractions, τ_0/τ_{fret}. The distribution of τ_0/τ_{fret} in different regions is shown far left. The locations of the maxima differ by only 10%, corresponding to a distance variation of about 2%. However, the variation in the intensity coefficients, a/b, is about 10:1.

The results show clearly that the variation in the single-exponential lifetime (Fig. 295) is almost entirely caused by a variation in the fraction of interacting proteins, *not* by a change in distance. In other words, interpreting variations in the single-exponential lifetime (or classic FRET efficiencies from steady-state experiments!) as distance variations leads to wrong results.

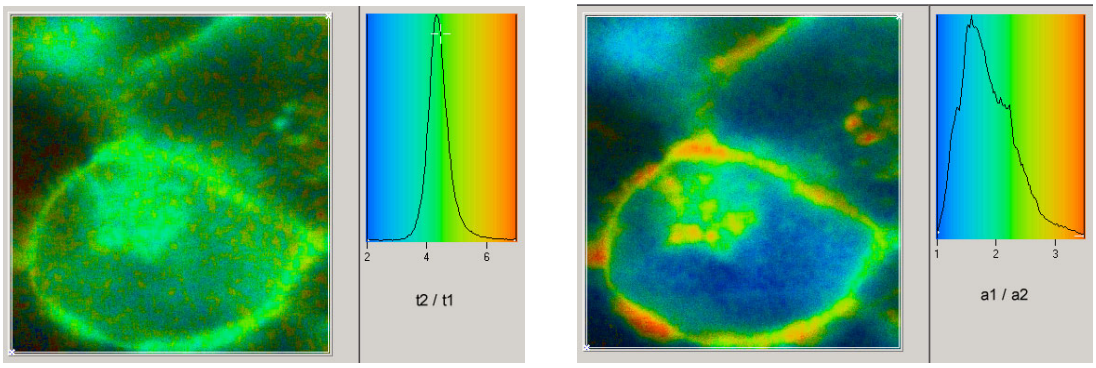

Fig. 298: FRET results obtained by double-exponential lifetime analysis. Left: Ratio of the lifetime components, t2/t1 = τ_0/τ_{fret}, Right: Ratio of the interacting and non-interacting donor fractions, a1/a2 = N_{fret}/N_0. Cells courtesy of Burkhard Wiesner, Leibniz Institute of Molecular Pharmacology (FMP), Berlin, Germany

Similar double exponential decay behaviour is commonly found in FRET experiments based on multi-dimensional TCSPC [11, 38, 40, 42, 71, 88, 122, 126, 280]. Double-exponential decay profiles have also been confirmed by streak-camera measurements [69, 70]. For many years, the double-exponential decay was discussed controversially. The discussion was enhanced by double-exponential decay behaviour found for some FRET donors themselves. Now there is no doubt any more that FRET induces a double-exponential donor decay, and that the components represent interacting and non-interacting donor fractions.

The fact that the slow decay component comes from the non-interacting donor can be exploited for FRET analysis: The lifetime of the slow component is the reference lifetime for the FRET calculation. The advantage is that this lifetime comes from the same cell and from the same pixels, and that it was measured simultaneously with the lifetime of the interacting donor. Possible variations by variable local environment have therefore no influence on the FRET result. Moreover, it can be expected that the slow lifetime does not vary noticeably throughout the cell. The slow lifetime can therefore often be used as a global parameter in the fit process [16].

Although the double-exponential approach yields good results it should be noted that FRET experiments can be more complicated than described above. There is the problem that a protein can be expressing (or be labelled with) several donor or acceptor molecules. The effect of multi-labelling is energy migration between the donors, and an increase in the energy transfer rate due to the presence of several acceptors. For physical background and possible pitfalls please see [216, 217, 358].

It should also be mentioned here that double-exponential FRET measurement faces the problem that the fluorescence decay of the unquenched donor itself is often multi-exponential. This happens especially for the CFPs and its variant, Cerulean. Strong multi-exponential behaviour can also be induced by fixation procedures (see Fig. 285) and by excessive photobleaching [178].

The situation can be complicated if the donor fluorescence is contaminated by autofluorescence [188]. The decay profiles of autofluorescence are multi-exponential, and can look very similar to the decay of the donor in a FRET system, see Fig. 306. Negative tests with unlabeled cells and with donor-only cells are therefore mandatory.

FRET results can also be biased by photobleaching or photoconversion of the fluorophores [178]. Even photo-induced changes in the protein conformation cannot entirely be excluded, see Fig. 307. In the last years, photo-induced artefacts have been reduced by better efficiency of the detectors, better efficiency of the microscope optics, and by new fluorescent proteins with higher photostability [109, 110].

FLIM-FRET experiments need not necessarily be performed in single cells. The same data analysis principles can, of course, be applied to fluorescence decay data obtained from protein or cell suspensions in cuvettes or micro-cuvettes [79, 164, 183]. The advantage of these measurements is that photobleaching is not a problem, the disadvantage is that only average FRET parameters over the whole volume of the cells and over a large number of cells are obtained. Usually, not all cells express the acceptor. Consequently, the result can be biased towards lower FRET efficiency, and a lower fraction of interacting proteins.

Using Information from the Acceptor Decay Function

There is continuous discussion about the shape of the acceptor decay function, whether it can be used to improve the accuracy of FRET measurements, and whether FRET results can be derived form an acceptor lifetime image. Fig. 299 shows how the acceptor decay function in an ideal FRET experiment should look like. Acceptor excitation occurs via the S1 state of the interacting donor molecules. The number of interacting donor molecules in the S1 state is represented by the fast donor fluorescence component. Consequently, this component acts as an excitation pulse to the acceptor. The acceptor fluorescence decay function should therefore have a slow rising edge with a time constant equal to the decay time of the interacting donor fluorescence.

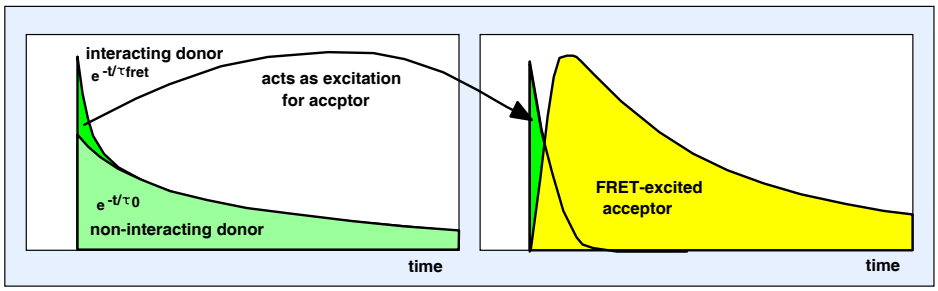

Fig. 299: Donor and acceptor decay functions expected in an ideal FRET experiment: The excitation of the acceptor comes from the interacting donor

However, nothing like this is observed in practical FLIM FRET experiments. Fig. 300 shows a lifetime image of the acceptor of the HEK cell shown in Fig. 295. The mean lifetime is between 2.3 and 2.6 ns. The fluorescence decay from the region of strong FRET has lifetime components of 2.2 ns and 3.2 ns. The shape is close to a single-exponential decay. There is neither a trace of a slow rise, nor is there a decay component with a negative amplitude.

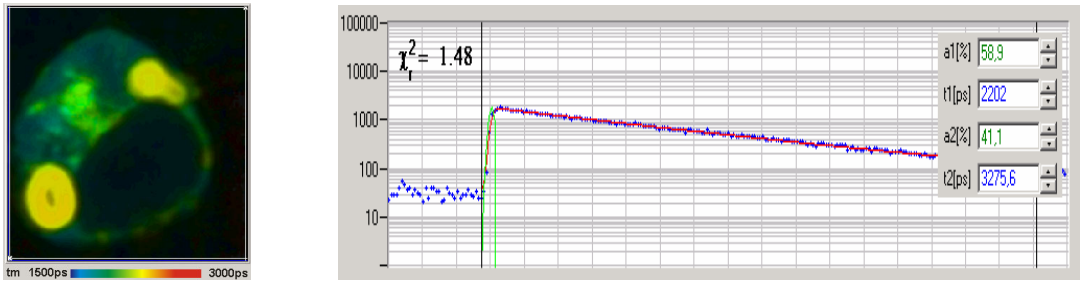

Fig. 300: Left: Acceptor lifetime image of the HEK cell shown in Fig. 295. Right: Acceptor decay function in region of strong FRET (right)

The explanation of the observed donor decay profile is in the fluorescence spectra. There is a strong overlap of the donor emission into the acceptor emission. The observed acceptor decay is therefore a sum of the donor emission overlapping into the acceptor spectrum, the decay of the FRET-excited acceptor, and a contribution from directly excited acceptor. This is in

agreement with the decay components shown in Fig. 300: The lifetimes of the decay components are close to the average lifetime of the donor, CFP, and the typical lifetime of YFP.

In CFP-YFP experiments the amount of donor fluorescence in the spectral range of the acceptor can be almost 50% of the observed acceptor fluorescence. Moreover, the decay time of the fast donor component is exactly the rise time of the FRET-excited acceptor. Both effects cancel, and the result is a near-single-exponential decay function, as shown in Fig. 301.

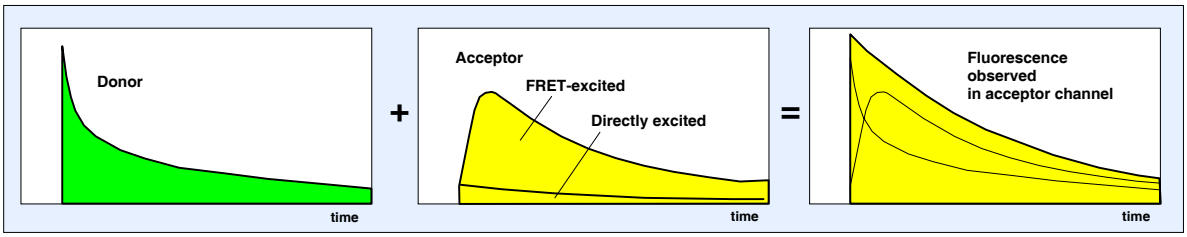

Fig. 301: The observed acceptor decay is a sum of FRET-excited acceptor fluorescence and donor fluorescence emitted in the spectral range of the acceptor.

The prospects of using the acceptor decay functions in FLIM FRET are therefore not good. It has been attempted to obtain additional FRET information from the acceptor emission measured simultaneously with the donor emission in a dual-detector TCSPC system [182]. An attempt was made in [43] to subtract the donor bleedthrough from the acceptor decay and to build up an acceptor lifetime image free of donor bleedthrough. The result showed indications of the slow-rising acceptor component but also a large amount of directly excited acceptor fluorescence. The slow rise of the acceptor fluorescence has been observed in [79] and [333]. These measurements were performed in protein solutions in cuvettes. The reason that the slow rise of the acceptor fluorescence stands out more prominently than in the FLIM data is possibly that the cuvette experiments used more restrictive filtering: [79] detected through a 557 nm filter, [333] in the 540 nm channel of a bh PML-16 multi-wavelength detector. Typical CFP / YFP beamsplitters used in microscopy split the signals at 510 to 520 nm and thus record more donor bleed-through.

Even if the FRET-excited component of the acceptor fluorescence is correctly extracted from the decay data as shown in [333], all these attempts are facing the same problems as intensity FRET: It is not possible to record the FRET-excited acceptor fluorescence without accurate correction of the donor bleedthrough and the contribution from directly excited acceptor fluorescence.

A more promising approach to the exploitation of the acceptor fluorescence is multi-wavelength detection [39, 47]. Reference spectra of the donor and the acceptor would be recorded, and the FRET fluorescence would be fitted by a model containing these spectra and the unknown intensity coefficients and lifetimes of the donor and the acceptor. Thus, multi-wavelength FLIM may lead to a combination of FLIM-based and sensitised-emission FRET techniques. A demonstration of the technique has been given in [72, 73, 74, 333].

Dark acceptors

An exciting possibility to improve FLIM FRET results is to use a dark acceptor. The advantage of this approach is that donor-acceptor pairs with almost ideal overlap of donor emission and acceptor absorption spectra can be selected. The FRET efficiency for a given donor-acceptor distance is therefore higher than for conventional FRET pairs.

The situation for the GFP-YFP pair is shown in Fig. 302. The figure shows that the pair would be almost impossible for use for conventional FRET: The emission of the GFP and the YFP

cannot be spectrally separated, and excitation of the GFP anywhere close to its absorption maximum would also excite a large amount of YFP. However, there is an excellent overlap between the GFP emission and the YFP absorption. With a dark YFP, the GFP emission can be detected, and the FRET efficiency determined by FLIM FRET. A dark YFP mutant (called resonance energy accepting chromoprotein, REACh) has indeed been developed, and the GFP- (dark)YFP pair been used for FRET experiments [143, 144, 261, 278].

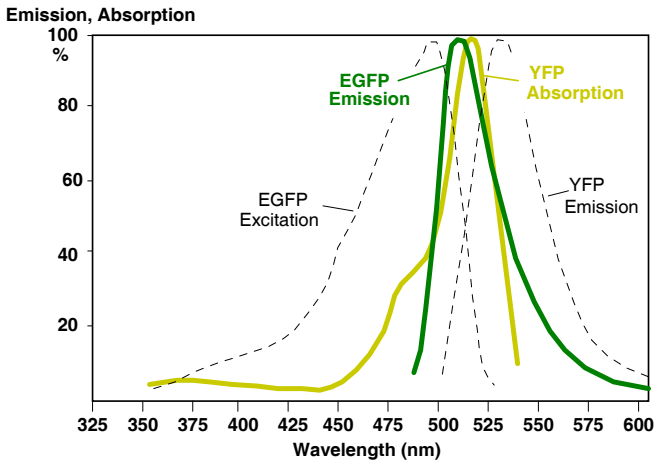

Fig. 302: Absorption and emission spectral of GFP and YFP, after [105]

One argument against FRET experiments with a dark acceptor is that the acceptor is not entirely free of fluorescence - the fluorescence is only strongly quenched. The donor emission would therefore be contaminated by an unknown amount of acceptor fluorescence. Such contamination may indeed exist. What happens in detail depends on whether the fluorescence of the acceptor itself is quenched dynamically or statically [226] is shown in Fig. 303, left and right. Dynamic quenching results in en extremely short fluorescence lifetime of the acceptor. The decay function of the FRET-excited acceptor is then identical with the decay component the interacting donor. Contamination would result in a slight over-estimation of the amount of interacting donor. Static quenching (if incomplete) would result in a weak acceptor fluorescence with the normal lifetime. The result would be contamination by a FRET-excited or directly excited acceptor decay, and thus an over-estimation of the non-interacting donor fraction. The size of both effects can be determined by recording FLIM of acceptor-only samples.

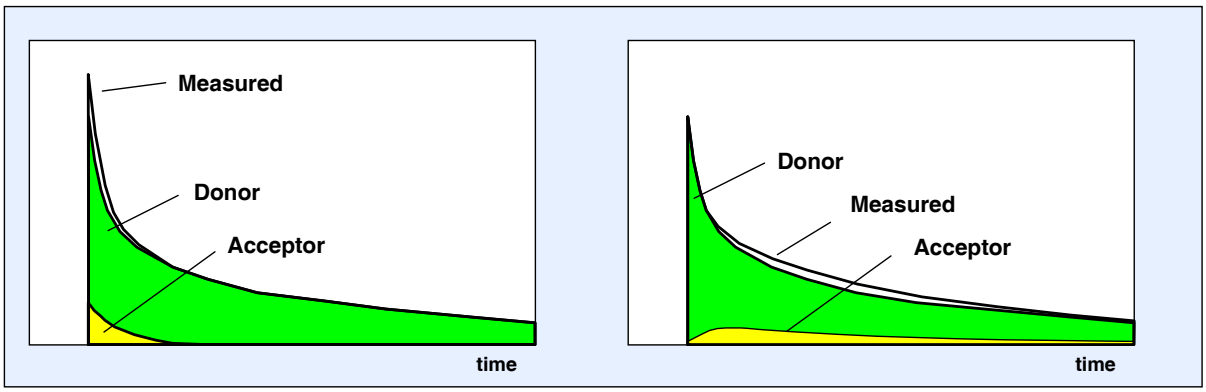

Fig. 303: Contamination by ‘dark’ acceptor fluorescence. Left: Acceptor quenched dynamically. Right: Acceptor quenched statically.

Another argument against dark-acceptor FRET is more serious: There is no way to prove that the cells are expressing the acceptor. If there is no acceptor FRET will not occur, even if the labelled proteins are perfectly interacting. Consequently, the *absence* of a FRET signature in the donor decay function is no prove of the absence of protein interaction.

FRET between Endogenous Fluorophores

There is a number of endogenous fluorophores with overlapping emission and absorption spectra. That means FRET can, in principle, occur between the fluorophores, and be exploitable to investigate interactions of the associated proteins. Serrano et al. used FRET from an amino acid (the donor) into tryptophane to detect structural heterogeneity [320]. Tryptophane can also be used as a FRET donor. The problem of these experiments is that amino acids or tryptophan must be excited deep in the UV, around 250 nm. The optics of a normal microscope and of the scan heads of normal laser scanning microscopes is transparent only down to about 360 nm. Li and Seeger therefore built a confocal UV microscope with 266 nm excitation wavelength, a PMH-100-6 detector and an SPC-630 TCSPC module. They were able to obtain decay curves from tryptophane, and show that the fluorescence lifetime decreases on interaction with other proteins [234]. There are currently attempts to reach tryptophane via three-photon excitation in multiphoton microscopes. The problem of this approach is that this wavelength excites NADH and FAD via two-photon excitation. Ar a given laser power, two-photon excitation is far more efficient than three-photon excitation. It can easily kill the cells as we have found in our own test experiments. Nevertheless, it has turned out that three-photon excitation of tryptophane - and the detection of its fluorescence - is possible. With UV-optimised optics in the detection beam path, hybrid detectors, and carefully adjusted laser power three-photon excited TCSPC FLIM images of tryptophane were obtained. Possible FRET would occur between the tryptophane and the bound component of the NADH. Indeed, FLIM experiments have shown a decrease in the tryptophane lifetime with the bound-unbound ratio of the NADH fluorescence [190, 278].

FRET in Diffraction-Limited Spots

Problems may occurs when FRET occurs in image details too small to be resolved in the optical microscope. To show up in the image at all, a sub-resolution structure must emit fluorescence at an intensity much higher than the environment. That means the fluorophore concentration in the structure itself must be very high. High concentration bears the risk of interaction of the donor molecules with several acceptors [217]. The FRET efficiency for a given donor-acceptor distance is then higher than expected. The second problem is on the detection side. The fluorescence decay function from a sub-diffraction structure will necessarily be contaminated by fluorescence from the closer environment. If there is no FRET in the environment (which is the purpose of the experiment) the FRET efficiency and the fraction of interacting proteins come out too low.

Typical cases are cell membranes or synapses between neurons. A beautiful FLIM FRET image of a live cultured neuron is shown in Fig. 304. FRET is expected to occur in synapses. As can be seen in the image on the left there are a large number of small spots with decreased lifetime. Magnified images of two typical details are displayed on the right.

The interpretation of such data is far more difficult than in a cell like the one shown in Fig. 314, page 201. The spots of decreased lifetime are hard to distinguish from photon-induced noise and from variation due to inhomogeneity of the local environment. Conclusions can only be made by correlating the spots of decreased lifetime with the morphology, by comparing a large number of measurements, and including negative tests with acceptor-free samples.

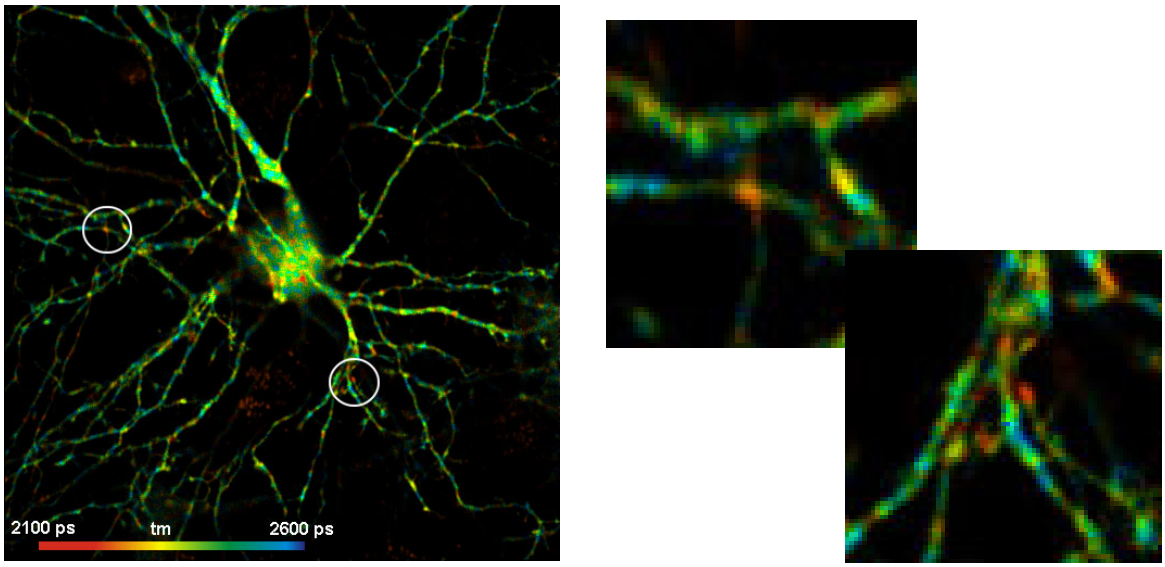

Fig. 304: Live cultured neurons. FRET expected in synapses. Left: Full image, interesting candidates marked. Right: Magnified images of details marked. Zeiss LSM 7 MP microscope with Simple-Tau 152 FLIM system and HPM-100-40 hybrid detectors. Analysis by SPCImage, incomplete decay model with two exponential components. Data courtesy of Inna Slutsky, University Tel Aviv.

FLIM FRET in synaptic structures has been published by Bosch et al. and by Fogel et al. Bosch et al. were not only able to detect protein interaction, they could even follow the reorganisation of post-synaptic substructures during long-term potentiation by time-series FLIM [80]. Fogel et. al. [132] used a combination of intensity FRET measurement, FLIM FRET measurement, and single-molecule imaging to show that the amyloid precursor protein homodimer constitutes a resynaptic receptor that transduces a signal from amyloid-beta peptides to glutamate release. Dore et al. and Murokashi et al. performed FLIM-FRET experiments in single dendritic spines [119, 261].

Homo FRET

The FRET technique described above is based on resonance energy transfer between *different* fluorophores. It should be mentioned, that FRET is also possible between *similar* molecules. Resonance energy transfer between similar molecules is called homo-FRET. Homo-FRET leaves the fluorescence decay profiles unchanged: The energy transferred from the first molecules to a second one is emitted by the second molecule, and the sum of the decay rates does not change. What changes, however, is the fluorescence anisotropy. Homo FRET has thus to be detected by comparing the intensities and decay profiles in two detection channels of perpendicular polarisation [263, 359]. This is possible by using a polarising beamsplitter in the detection beam path. In most scanning microscopes these are not available as standard parts. Thaler et al. therefore detected through the condenser beam path of an LSM 510 NLO. Their paper on structural rearrangement of CaMKIIα catalytic domains is based on homo FRET and can be recommended as an amazing piece of scientific detective work [344].

Practical Hints for FRET Measurements

Multi-Exponential Decay of the Free Donor

Double-exponential FRET measurements are faced with the problem that the fluorescence decay of the unquenched donor itself can be multi-exponential. This happens especially for the CFPs and, at a smaller extend, Cerulean. CFP has two lifetime component of about 1.3 ns and

2.9 ns with an amplitude of 20 to 40% and 60 to 80%, respectively [42]. Sarkar et al. [309] found an almost similar composition (60% of 3.7 ns and 40% of 1.5 ns) for Cerulean excited at 405 nm. Interestingly, there is no trace of a second component in our own data from live cells, see Fig. 285, left. It is therefore possible that the composition of the decay depends on the molecular environment, or on the excitation wavelength.

Fortunately, in FRET experiments the fast lifetime component in the donor decay is usually in the range of 400 to 800 ps. Under these conditions a double-exponential fit routine tends to combine the 1.3 ns and the 2.9 ns component into one component of about 2.5 ns. Thus, the interacting and non-interacting donor fractions can still be distinguished.

Almost ideal single-exponential decay profiles are obtained from GFP. GFP or EGFP are therefore increasingly being used as FRET donors.

Please note that strong multi-exponential behaviour can be induced by fixation procedures. The frequent complaints about strongly multi-exponential donor decay probably result from measurements of fixed samples, see below.

Live Samples versus Fixed Samples

FRET measurements aim at measuring changes in the conformation and binding of proteins. That means, that the molecular structure of a sample must be preserved during sample preparation. In other words, FLIM measurements normally have to be performed on live cells or live tissue. Fig. 285 shows what can happen if this simple fact is ignored. Both images show cells of the same type, transfected with Cerulean. The excitation wavelength was 445 nm, the detection wavelength 480±20 nm. The left image was obtained from a live cell, the right image from a fixed cell. Both cells were analysed by a double-exponential model.

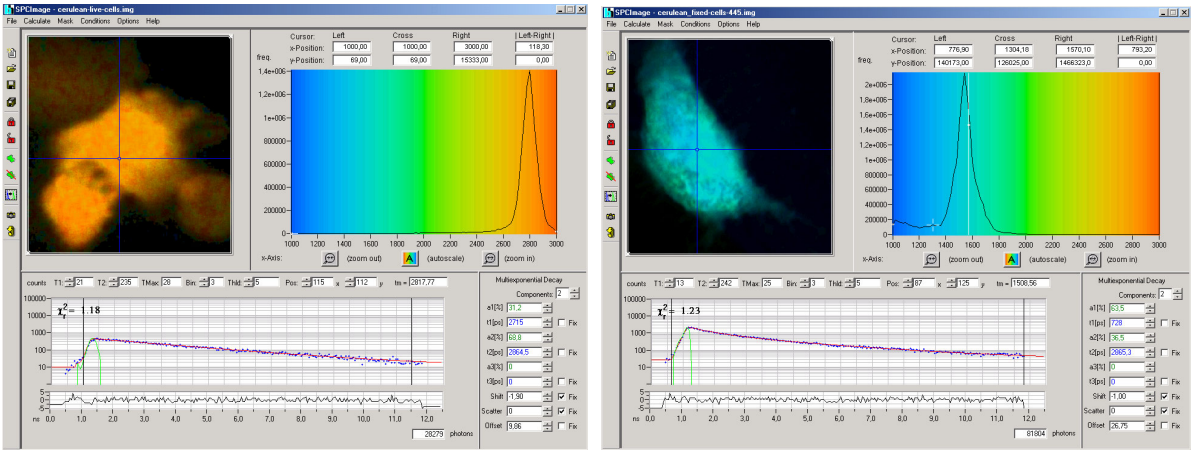

Fig. 305: Lifetime differences between a live cell (left) and a fixed cell (right). Colour-coded lifetime image, histogram of lifetimes over the pixels, decay curve in selected spot of the image, excitation 445 nm. Both cells are expressing Cerulean, without any FRET acceptor. Nevertheless, the fixed cell shows a decay profile typical for FRET.

The live cell delivers two almost identical lifetime components. This is a clear indication that the decay is almost perfectly single-exponential. The lifetime is about 2.8 ns. This is exactly what one would expect for a cell expressing Cerulean alone.

The fixed cell (Fig. 285, right) shows a strongly double-exponential decay profile, with 60% of 770 ps and 40% of 2.8 ns. The amplitude-weighted mean lifetime is around 1.56 ns. Moreover, the lifetime histogram shows a broad background of shorter lifetimes from the embedding medium. No matter what kind of experiment this result would be used for, it would lead

to significantly wrong results. Consider a FRET experiment: The decay profile of the fixed Cerulean cell is similar to the decay profile of a cell showing FRET, compare Fig. 297. An inexperienced user may interpret the decay profile as 60% of interacting proteins, with a FRET efficiency of 0.725. The average FRET efficiency would be 0.44. However, the cell does not contain an acceptor, and consequently, cannot do any FRET.

Similarly wrong lifetimes and decay profiles are found also for other fluorescent proteins in fixed samples. It appears likely that the frequent complaints about strong multi-exponential decay of CFPs at some extend originate from measurements on fixed samples.

Autofluorescence

A frequent pitfall of FRET experiments is autofluorescence. If the cells are not expressing the fluorophores as expected autofluorescence dominates the FLIM signals. Autofluorescence has a fast and a slow decay component. The shape of autofluorescence decay functions can be very similar to those of FRET, see Fig. 306. FLIM can help to identify autofluorescence problems: If the slow decay component (circled) is not as expected for the free donor something must be wrong with the sample. However, even this is not sure. If autofluorescence wants to fool you it will, as can be seen in Fig. 306, right. Negative tests with un-transfected cells and with acceptor-free cells are therefore mandatory for proving the relevance of FRET results.

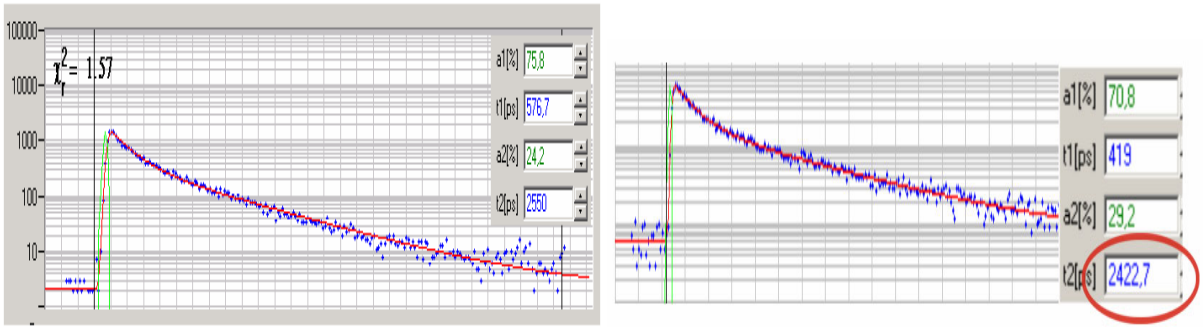

Fig. 306: Fluorescence decay from the donor of a CFP-YFP FRET system (left) and fluorescence decay of autofluorescence

Photobleaching

Photobleaching acts differently on the interacting and the non-interacting donor fraction. The non-interacting donor component photobleaches faster, so that the fraction of interacting donor (and thus the conventional FRET efficiency) is biased towards higher values. It is also possible that the acceptor photobleaches. In that case, photobleaching decreases the fraction of interacting donor. Moreover, photobleaching can create photoproducts that are fluorescent. Emission from these compounds can change the composition of the decay profiles unpredictably [178].

As a rule of thumb, the count rates should not decrease by more than 20% during the measurement. If you notice excessive photobleaching, try with a lower laser power and a correspondingly longer acquisition time. In one-photon systems, you may use a larger pinhole and thus trade count rate against depth resolution. Even if you have to sacrifice a number of cells for these experiments the higher number of photons obtained at less photobleaching pays off at the end.

It should also be taken into regard that the exposure may induce real changes in the protein conformation in the cells. A possible example is shown in Fig. 307. The images shows a live-cell sample expressing interacting proteins fused with CFP and YFP.

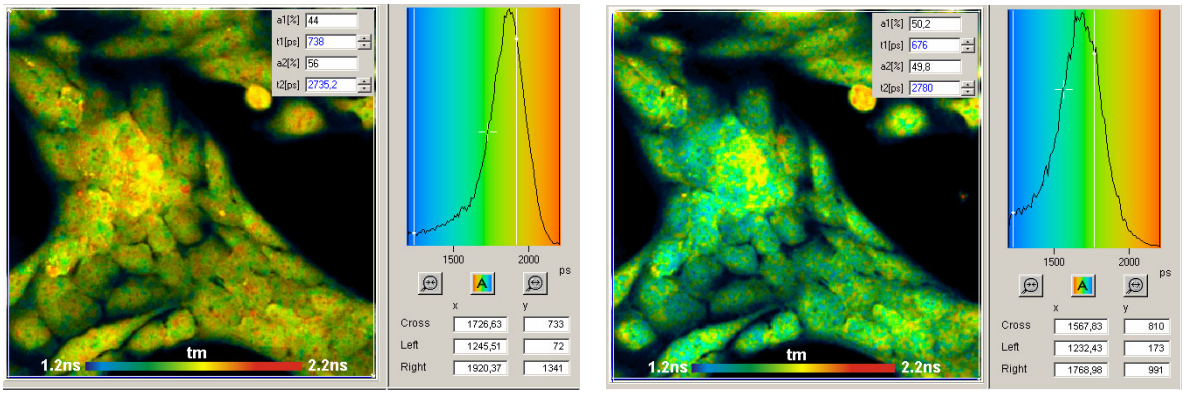

Fig. 307: Two FLIM FRET measurements of the same sample, lifetime images and lifetime histograms. Left: Initial recording, acquisition time 30 seconds. Right: Second recording, acquisition time 30 seconds, after 90 seconds of total exposure. Insert: Amplitudes and lifetimes of the decay components. Analysis by bh SPCImage, incomplete decay model with two exponential components

Two-photon excitation at 860 nm was used, the laser power regulator of the microscope was set to 4%. This is a power commonly used in two-photon live cell imaging. Both images were recorded at the donor emission wavelength. After getting the sample into focus, a 30 seconds FLIM recording was taken. Then the scanning was continued for another 60 seconds, and another 30 second image was taken. As can be seen from the images, the lifetime (amplitude weighted lifetime, tm) in the second recording is significantly shorter. The shorter t_m comes from a larger amplitude and a shorter lifetime of the fast decay component. The slow decay component remained virtually unchanged. This is exactly what should be expected if the protein interaction had become stronger. This interpretation may be a bit speculative, but is shows that real changes in the sample should be considered at least as a possibility.

Photobleaching, and, possibly, photo-induced changes in the samples, has been a frequent problem of FRET measurements in early FLIM systems. These systems used PMTs with conventional photocathodes and, in many cases, inefficient ports of the microscopes. In the last years the photobleaching problem has been reduced by hybrid detectors [50] and highly efficient microscope optics. There is also a continuous development of new photostable fluorescent proteins which further reduce photobleaching artefacts [109, 110].

FRET Literature

An enormous amount of FRET papers based on the bh FLIM technique has been published in the last few years. An overview about FRET techniques, their applications and the related pitfalls is given in [358]. A detailed description of a TCSPC-FLIM-FRET system is given in [122]. The system was used for FRET between ECPF-EYFP and FM1-43 - FM4-64 in cultured neurones. A number of papers give a general characterisation of TCSPC-FLIM FRET for monitoring protein interactions [71, 97, 98, 280, 326]. A combined FLIM-FRET microscope / endoscope system is described in [140]. The system simultaneously scans FLIM images through the beam path of an inverted microscope and records fluorescence from the back of the sample through a fibre bundle. Elder et al. reviewed different methods of FRET signal normalization and verified them by TCSPC FLIM [124].

A comparison of the accuracy of FRET measurements by different techniques has been given by Pelet et al. [274]. The authors compared FLIM, spectral imaging, and two-channel intensity imaging with calibration of excitation and emission crosstalk. For the individual measurements they used identical optical paths, comparable data acquisition times and comparable

fluorescence intensities. It turned out that the FRET results obtained from the FLIM data had a three-times smaller standard deviation than those obtained from the dual-channel and spectral measurements. Sun & Periasamy compared conventional FRET efficiencies obtained by filter-based FRET measurements with FRET efficiencies obtained by FLIM FRET [340] and found that additional correction is needed for filter-based measurements.

The construction of FRET standards and their verification by FLIM measurement are described in [90, 215]. Although FLIM FRET actually does not need calibration the standards are required to verify and compare the results obtained by different FRET techniques.

There is a number of FRET applications which are directly related to clinical research [247]. Because FRET yields information about protein interaction it can be used to investigate the formation - and possible dissolution - of amyloid plaques of Alzheimer's disease [11, 12, 62, 63, 64, 163, 176, 189, 236, 237, 353]. Mechanisms of Huntington disease (a progressive neuro-degenerative disorder) were investigated in [136] and [262].

FLIM FRET in synaptic structures has been published by Bosch et al., Fogel et al. and Ueda et al. [80, 132, 351, 352]. These experiments are difficult because FRET occurs in sub-resolution volumes of the sample. The effects are therefore difficult to detect, see above, 'FRET in Diffraction-Limited Spots'. Bosch et al. were not only able to detect protein interaction, they could even observe the re-organisation of post-synaptic substructures during long-term potentiation by time-series FLIM [80]. Fogel used a combination of intensity FRET measurement, FLIM FRET measurement, and single-molecule imaging to show that the amyloid precursor protein homo-dimer constitutes a resynaptic receptor that transduces a signal from amyloid-beta peptides to glutamate release.

Kelleher et al. demonstrated deep tissue FLIM-FRET in cancer cells and animal models. Two-photon excitation was used to obtain FRET images from layers as deep as 100 µm [197].

Another potential FRET application is the investigation of infection mechanisms. The technique was demonstrated by Ghukasyan et al. for the infection of HeLa cells with enterovirus 71 [153]. Jeshtadi et al. [186], Danquah et. al. [106] and Cheung et al. [99] used FRET to investigate interaction of virus proteins with proteins of the host cell. The FRET pair was GFP-DsRed. The spreading of viruses in plant cells was studies by Amari et al. [5], fungus infection of plant cells by Shen et al. [321].

Almost all the FLIM-FRET applications are more or less related to interaction interactions of various proteins or to protein organisation [2, 3, 4, 1, 69, 71, 77, 81, 80, 119, 132, 138, 139, 142, 149, 159, 184, 187, 193, 199, 201, 218, 221, 238, 239, 240, 242, 261, 264, 275, 287, 295, 308, 312, 318, 319, 330, 346, 360, 372]. Monitoring HIV-1 Protein Oligomerization by FLIM FRET was described in [288]. Protein interaction studies include detection of enzymatic activity in neuronal micro-compartments by FRET [370], Na^+ channels [251], or intracellular transport mechanisms and membrane trafficking [108, 255, 289]. Rochel et al. used FRET to study the role of DNA in the spatial organisation of nuclear hormone receptors (NHRs) [298]. Interactions between the PCK and NKκB signalling pathways have been investigated in [257]. [334] investigated the association of protein kinase C alpha (PKCα) with caveolin. FRET between GFP and RFP and FRET cascades from GFP via Cy3 into Cy5 are demonstrated in [281] and [1]. The agglutination of red blood cells by monoclonal antibodies was studied using FRET between Alexa 488 and DiI [296]. Interaction of the neuronal PDZ protein PSD-95 with the potassium channels and SHP-1-target interaction were studied in [69, 71]. Interaction of αB-crystallin with focal adhesion kinase (FAK) was investigated in by Pereira et al. [279] and shown to confer protection to FAK against calpain mediated proteolysis in cardiomyocytes. It has also been shown that conformational changes of proteins in cells can be

monitored by FLIM-FRET [88, 237]. Tynan et al. and Martin-Fernandez used FRET to gain insight into the structure of the human epidermal growth factor (EGFR) [243, 350]. Mergenthaler et al. investigated the function of mitochondrial HKs in different states of metabolic deprivation during hypoxia and hypoglycemia [250]. A new Ras sensor was developed and characterised by Oliveira and Yasuda [265].

A variety of papers are devoted to the conformation and interaction of SNARE proteins and mechanisms modulating their interactions [222, 247, 268, 289, 290, 291, 325, 354]. In [290] double-exponential FRET was used to distinguish interacting and non-interacting protein fractions. Studies of the interaction dynamics on the millisecond time scale are described in [291].

Ariola et al. used a Bodipy-cholesterol derivate (Bdp-Chol, donor) and Dil-C12 (acceptor) to probe fluidity and lipid order in cell membranes [7]. They found a reduction in lifetime of the Bdp-Chol in ordered domain which they attributed to FRET. The results were confirmed by anisotropy decay measurement.

The influence of shear forces on protein conformation was investigated in [89, 92, 373]. The authors used a micro-fluidic setup to induce dynamic forces on the cells. The setup was placed under a microscope and illuminated by a frequency-doubled Titanium-Sapphire laser. The donor fluorescence was detected by a bh PML-16 multi-wavelength detector with polychromator, and recorded be an SPC-630 TCSPC module. A similar setup was used to study the influence of oxygen concentration [374]. The Oxygen supply was turned on and off by starting and stopping the flow in the cell. The oxygen concentration was monitored via the emission intensity of a phosphorescence probe.

FRET between ECFP and EYFP in plant cells was demonstrated in [78]. FRET measurements in plant cells can be difficult because of the strong autofluorescence of the plant tissue. The authors showed that two-photon excitation can be used to keep the autofluorescence signal at a tolerable level. The autofluorescence problem has also been solved by using the GFP Mutant TSapphire and the DsRed Variant mOrange as FRET donor and acceptor, respectively [17]. Protein interactions upon intrusion of fungal pathogens into plant cells were investigated in [83, 76, 321]. Interactions between Golgi tethering factors and small GTPases was studied by Osterrieder et al. [267].

There is a continuing search for new FRET pairs with higher photostability, better overlap of donor emission with acceptor absorption bands, and (important for steady-state FRET techniques) less donor and acceptor bleedthrough. Please see [17, 109, 110, 339] for new fluorescent proteins for FLIM FRET and their characterisation. An interesting approach is the use of a GFP as a donor and a dark YFP as an acceptor [143, 144].

It is also attempted to use quantum dots or combinations of quantum dots (as donors) and fluorescent proteins [248] or quantum dots and metal-organic complexes [331] as FRET partners. Spectroscopically, quantum dots make excellent FRET donors and acceptors. The photostability is excellent, and almost any absorption and emission wavelength can be obtained. The drawback is that quantum dots cannot be as easily be linked to target proteins as fluorescent proteins can.

Autofluorescence

Biological tissue contains a wide variety of endogenous fluorophores [210, 294, 314, 357]. So far, autofluorescence measurements of cells and tissue have been performed mostly by spectrally resolved imaging techniques. The problem of these techniques is that the emission and excitation spectra of the endogenous fluorophores are broad and poorly defined. Many of the fluorophores are mixtures of closely related compounds. The shape of the spectra can therefore not be considered constant. Moreover, absorbers present in the tissue may change the apparent fluorescence spectra. It is therefore difficult to unmix the fluorescence components by their emission spectra alone. The most serious drawback of purely spectral techniques is that different binding states of fluorophores cannot be distinguished.

Fluorescence lifetime imaging is likely to improve the contrast of separation of the different fluorophores. The most important argument for using lifetime imaging is, however, that the lifetimes of the dominating fluorophores depend on local environment parameters, such as binding to proteins, pH, or oxygen saturation, and on the binding to proteins. Autofluorescence lifetime detection therefore not only adds an additional separation parameter but also yields direct information about the metabolic state and the microenvironment of the fluorophores [68, 224, 226, 272, 314, 323, 324, 356].

Moreover, autofluorescence imaging has benefits in cases when the reaction of tissue to optical radiation is to be investigated, such as tumor induction by UV irradiation. Such experiments forbid the use of exogenous fluorophores because energy or electron transfer from the fluorophores to the proteins can induce unpredictable photoreactions. Moreover, FLIM is currently being introduced as a clinical diagnostics technique [210, 212, 313, 314]. In these applications the application of exogenous fluorophores is normally impossible.

The use of fluorescence-lifetime variations is especially promising for NADH and FAD. These coenzymes are involved in the electron transfer mechanism of the cell metabolism. Both NADH and FAD form redox pairs. NADH is fluorescent in its reduced form but loses fluorescence when oxidised. FAD is fluorescent when oxidised, and loses fluorescence when reduced. The fluorescence intensities of NADH and FAD therefore change with the redox state of the tissue [93, 94].

Approximate excitation and emission spectra of NADH and FAD are shown in Fig. 308. The spectra were taken from [314] and [226]. The figure shows that the best excitation wavelength for NADH is around 360 nm.

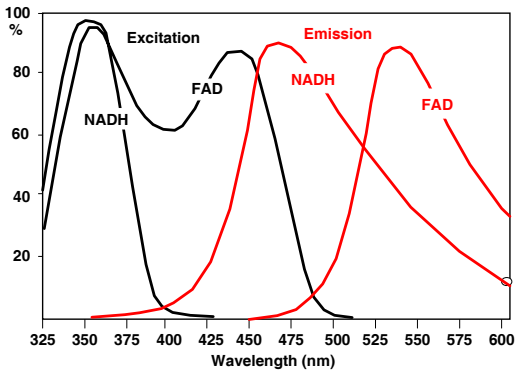

Fig. 308: Excitation spectra (one photon) and emission spectra of NADH and FAD. After [314] and [226].

Strong excitation can be achieved by the DCS-120 WB version and a 375-nm laser. Nevertheless, sufficient signal can be obtained also with excitation at 405 nm. A possible problem is that FAD is excitated more efficiently at this wavelength, so that contamination of the NADH

signal with FAD fluorescence cannot be excluded. Another way is to use two-photon excitation with the DCS-120 MP system. NADH can then be reached by 750 nm excitation wavelength.

It is known that the fluorescence lifetimes of NADH and FAD depend on the binding to proteins [224, 226, 272]. Unbound NADH has a fluorescence lifetime of about 0.4 ns. When NADH binds to proteins the lifetime typically increases to about 1.2 ns [226]. However, the bound-NADH lifetime depends on the proteins, and can reach 4 to 5 ns [226]. For FAD the effect of binding is opposite: Bound FAD has a lifetime of a few 100 ps, unbound FAD of a few ns.

An example of an autofluorescence image excited at 405 nm is shown in Fig. 310. The multi-exponential decay behaviour is clearly visible (see decay curves on the right), and both the amplitude-weighted lifetime and the intenisty contained in the slow and fast decay component shows substantial variation over the images.

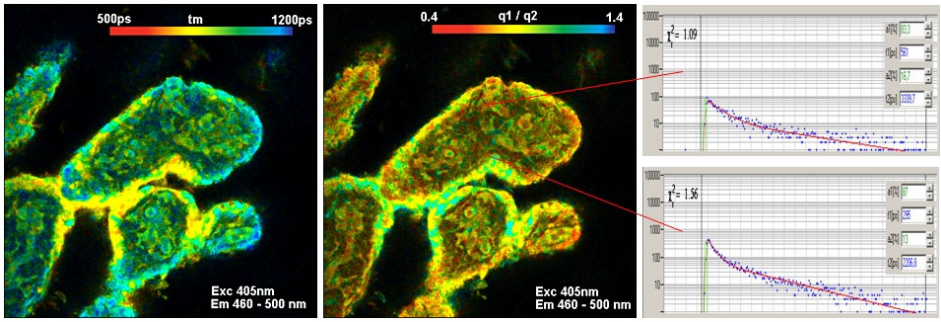

Fig. 309: Pig skin sample excited at 405 nm, detection from 460 to 500 nm. Double-exponential fit. Left: Amplitude-weighted lifetime. Middle: Intensity ratio of fast and slow decay component. Right: Decay curves in two

The fact that the NADH and the FAD fluorescence changes with the redox state and the binding makes it a sensitive indicator of metabolic changes. An excellent overview is given by Chorvat and Chorvatova [103]. Ghukasyan and Kao [154] have shown that the NADH decay parameters, in particular amplitudes of the fast and slow lifetime components, are indicators of physiological and pathological states of the cells. Bird et al. used a similar approach for metabolic mapping of human breast cells [68]; Skala et al. compared normal and precancerous epithelia [323, 324].

For autofluorescence imaging it is desirable to acquire fluorescence lifetime information without sacrificing the spectral resolution of the traditional autofluorescence techniques [101, 102, 103]. Autofluorescence FLIM measurements are therefore normally performed with several detectors or with the MW-FLIM multi-wavelength detector. An example of a spectrally resolved autofluorescence FLIM measurement is shown in Fig. 310.

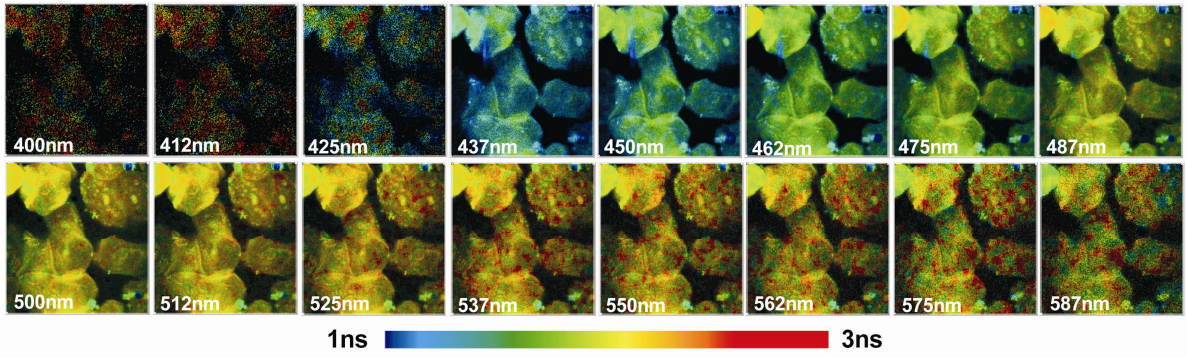

Fig. 310: Multi-wavelength lifetime image of the autofluorescence of human epithelium cells. DCS-120 scanner with MW-FLIM detector, excitation wavelength 405 nm, detection wavelength 400 nm to 587 nm.

The images were analysed by a double-exponential model. The lifetimes shown in Fig. 310 are the intensity-weighted average of the decay components of the double-exponential fit. A binning factor of 5, i.e. binning of 11x11 pixels was used in the analysis. The high binning factor is justified by the large zoom and the correspondingly large oversampling factor of the images (see 'Binning Decay Data', page 229).

As expected, the fluorescence decay profiles of autofluorescence deviate strongly from a single-exponential decay. Fig. 311 shows a decay curve from a 20 x 20 pixel area in the centre of the 450 nm window of Fig. 310.

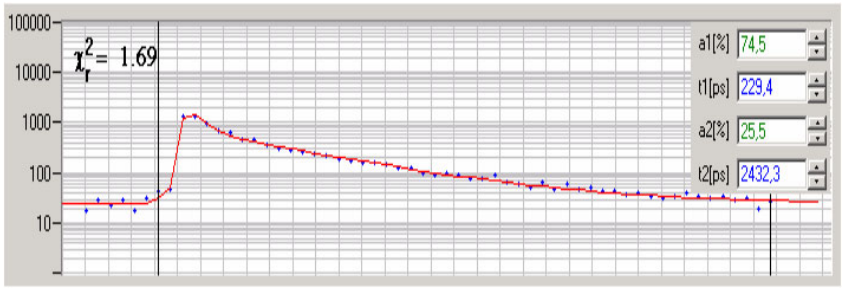

Fig. 311: Fluorescence decay curve of a 20 x 20 pixel area in the centre of the 475 nm window of Fig. 310.

The decay function can be approximated at satisfactory quality by a double-exponential decay model. It contains a fast component of 229 ps and a slow component of 2.43 ns, with amplitudes of 74.5 % and 25.2 %, respectively. The composition of the decay shown in Fig. 311 is typical of autofluorescence measurements. It is likely that the fast component originates from unbound NADH and bound FAD while the slow component comes from bound NADH and unbound FAD. The large amplitude and the wide spacing of the decay times makes double-exponential analysis feasible. In fact, a double-exponential model often delivers a more stable fit of autofluorescence decays than a single-exponential one.

The double-exponential data can be used to obtain images of the relative amplitudes or relative intensities of the lifetime components. An example is given in Fig. 312. The figure shows the relative intensities, i.e. the integrals of the photon numbers, contained in the fast lifetime component.

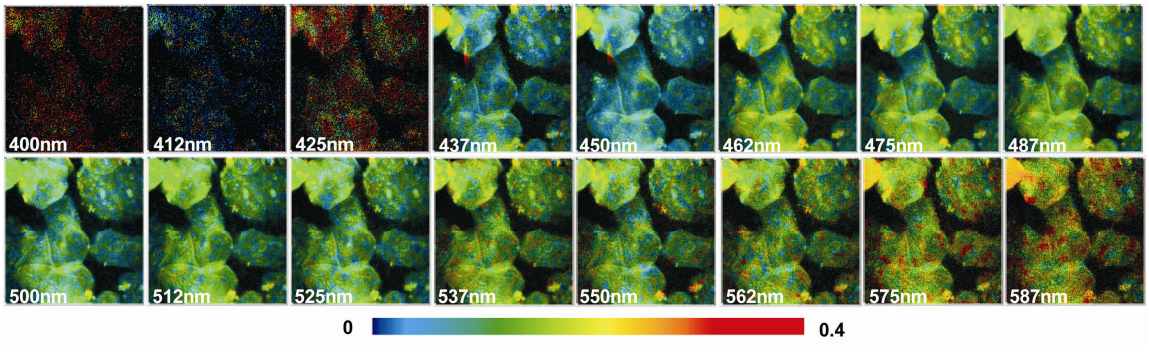

Fig. 312: Relative intensity contained in the fast decay component

Autofluorescence FLIM is often performed at relatively thick tissue, or even at living organisms. It is therefore a frequently asked question how deep in tissue a confocal FLIM system can produce useful images. Of course, one-photon confocal FLIM cannot compete with multiphoton NDD FLIM [23, 26]. Nevertheless, with the base version of the DCS-120 reasonable images are obtained up to a depth of about 50 µm. Fig. 313 shows a z stack of lifetime images taken from pig skin. The z step width was 4 µm, the whole stack is 52 µm deep.

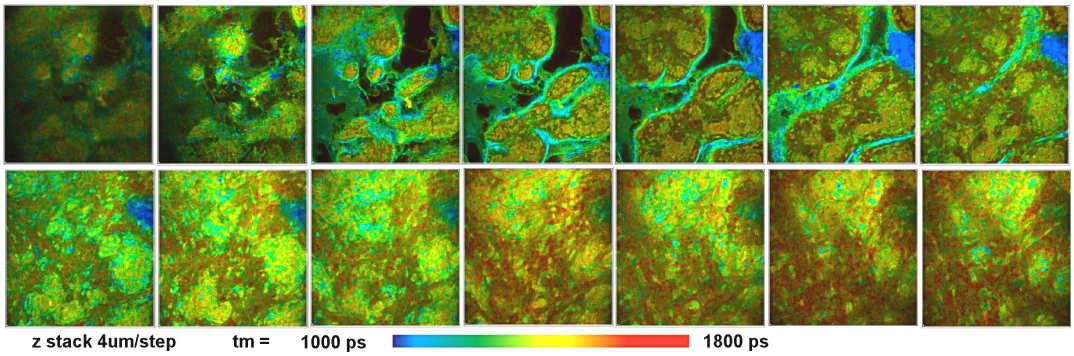

Fig. 313: Z stack FLIM of pig skin, 4µm per step. DCS-120 with Zeiss Axio Observer Z1, water C apochromat 63x NA=1.2, excitation 473 nm. Image size 256x256 pixels, 256 time channels.

What can be achieved in practice depends, of course, on the scattering and absorption coefficients of the tissue. The image quality in deeper layers also depends on the match of the refractive index of the tissue and the refractive index the lens is designed for. The refractive index of tissue is closer to the refractive index of water than of oil. Therefore water immersion lenses usually yield better images than oil immersion lenses.

The practical interpretation of fluorescence lifetime autofluorescence data is still subject of investigation. Full exploitation of multi-wavelength autofluorescence FLIM data would require a global fit with a suitable model that includes the effective spectra of the expected fluorophores. The task is extremely difficult because many of the endogenous fluorophores are in fact mixtures of slightly different compounds, with different absorption and emission spectra, and lifetimes [103, 314]. Moreover, there may be absorbers of unknown absorption spectra, inhomogeneous distribution, and unknown concentration in the tissue. Nevertheless, there is currently a number of approaches that are likely to solve at least a part of the problem [101, 102, 103, 284]. Further improvement can probably be achieved by excitation wavelength multiplexing.

Despite of these difficulties, there is an increasing number of exciting results. Schweitzer et al. used FLIM to investigate the autofluorescence of the fundus of the human eye in vivo. They were able to relate the lifetime components of a triple-exponential decay to different anatomic structures in the retina and the lens [314]. Moreover, they found a close relation of FLIM data to age-related macula degeneration [313]. Wu & Qu demonstrated that the fluorescence excited at 405 nm is sensitive to the cellular metabolism. Also here, different fluorescence components could be related to different tissue structures [368].

Ghukasyan and Kao [154] have shown that the NADH decay parameters, in particular amplitudes of the fast and slow lifetime components, are indicators of physiological and pathological states of the cells. Bird et al. used a similar approach for metabolic mapping of human breast cells [68], Skala et al. in normal and precancerous epithelia [323, 324]. Kantelhardt et al. and Leppert et al. found significant lifetime changes in mouse glioma [192, 230].

König et. al. used two-photon excitation and single-wavelength FLIM to record depth-resolved images of human skin [209, 210, 211]. These developments have already resulted in clinical applications [212, 214], see also bh TCSPC Handbook [55].

Plant Physiology

Plant tissue contains a large number of endogenous fluorophores. In practice the fluorescence is dominated by the fluorescence of chlorophyll and the fluorescence of flavines. The flavines emit in a broad range from 480 to more than 600 nm. Chlorophyll is excited at any wavelength throughout the visible spectrum and emits a strong fluorescence signal around 700 nm.

Multi-wavelength FLIM images of a moss leaf recorded with the bh multi-spectral FLIM system are shown in Fig. 314.

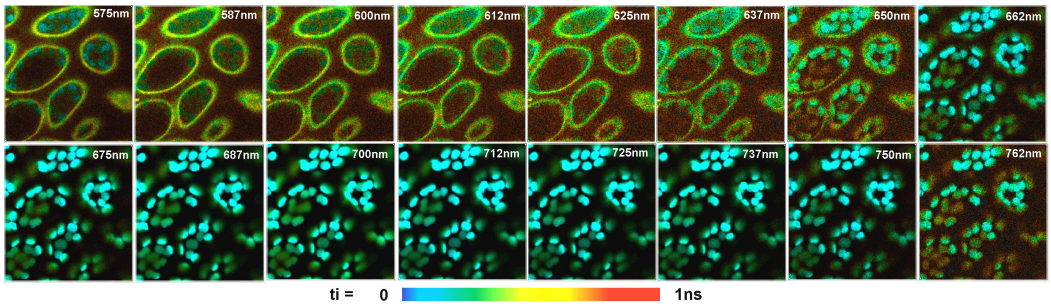

Fig. 314: Multi-spectral FLIM of plant tissue. Moss leaf, DCS-120, excitation at 405 nm, wavelength from 575 nm to 762 nm. Amplitude-weighted mean lifetime of double-exponential fit. Intensity normalised to brightest pixel of each wavelength interval. Image size 256x256 pixels, 64 time channels, 16 wavelength channels.

The fluorescence of chlorophyll competes with the energy transfer into the photosynthesis channels. Thus, the fluorescence lifetime is a sensitive indicator of the photosynthesis efficiency. The fluorescence lifetime of the chlorophyll in live plant tissue not only depends on the state of the tissue but also on the light intensity, and the time of exposure.

The changes in the fluorescence intensity of chlorophyll with the exposure to light have been found 1931 by Kautsky and Hirsch [195]. The effects have been termed fluorescence induction, fluorescence transients, or Kautsky effect [160, 161, 245]. When a dark-adapted leaf is exposed to light the intensity of the chlorophyll fluorescence starts to increase. After a steep rise the intensity falls again and finally reaches a steady-state level. The rise time is of the order of a few milliseconds to a second, the fall time can be from several seconds to minutes.

The initial rise of the fluorescence intensity is attributed to the progressive closing of reaction centres in the photosynthesis pathway. Therefore the quenching of the fluorescence by the photosynthesis decreases with the time of illumination, with a corresponding increase of the fluorescence intensity. The fluorescence quenching by the photosynthesis pathway is termed ‘photochemical quenching’. The slow decrease of the fluorescence intensity at later times is termed ‘non-photochemical quenching’. It is believed that it is a mechanism the plant uses to protect itself from photodamage.

Both the photochemical and the non-photochemical quenching transients in a single spot of a leaf can easily be measured by TCSPC [45, 55]. While recording photochemical quenching requires repeated triggered accumulation non photochemical quenching can be recorded in single simple time series of recordings. A non-photochemical fluorescence transient of a leaf is shown in Fig. 315. From left to right, the behaviour of a fresh leaf, a faded leaf, and a dried leaf are shown. The differences between leaves of different health state are striking. In fact, the differences in the dynamic behaviour of the fluorescence lifetime are much larger than the differences in the average (time-integrated) lifetime of the leaf.

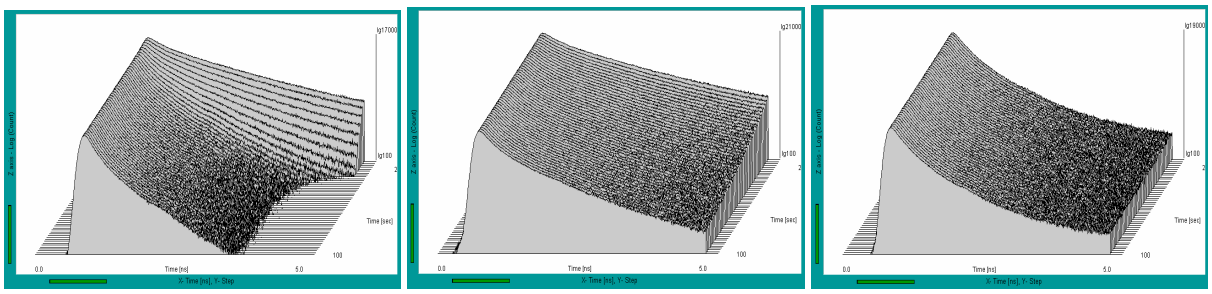

Fig. 315: Sequences of fluorescence decay curves measured at a leaf after start of illumination. Left to right: Fresh leaf, faded leaf, dried leaf. Time per curve 2 seconds, logarithmic intensity scale. The sequence starts from the back.

Non-photochemical transients can be measured by recording a conventional FLIM time series [194], see page 106, by a mosaic FLIM time series [34, 335] see page 113, or by FLITS [54], see page 132. For correct recording of the chlorophyll transient it is important that the FLIM sequence is obtained from a sample region that has not been exposed to the laser before. If the fast preview is used to adjust the focus we recommend to shift the sample by a small amount before the time series is started. When you are ready to start the experiment, start the measurement first, and then the scan. The sequence of actions is essential because the scan turns on the laser and thus synchronises the start of exposure with the FLIM time series.

A typical result is shown in Fig. 316. The acquisition time per image was 1 second, the image size 256 x 256 pixels x 64 time channels.

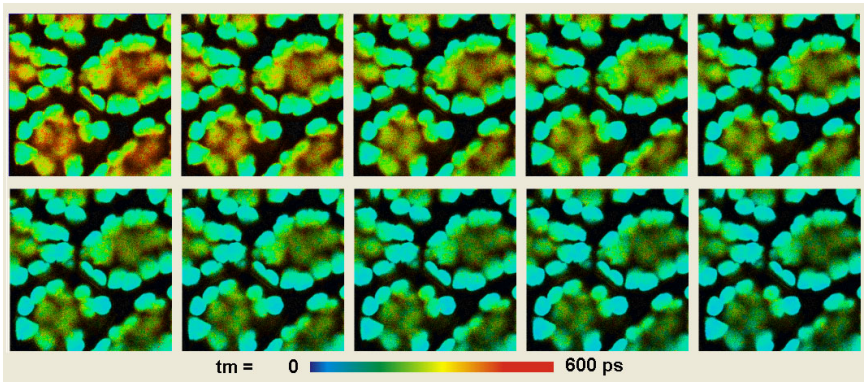

Fig. 316: Change of the fluorescence lifetime of chlorophyll with time of exposure. Moss leaf, 1-photon excitation at 445 nm, 256x256 pixels. SPC-150 autosave time-series, 1 image per second. Analysed by bh Optispec data analysis, intensity-weighted lifetime of double-exponential fit, blue to red corresponds to lifetime range from 200 to 400 ps

The illumination by the laser initiated an increase in non-photochemical quenching. The result is a decrease in the fluorescence lifetime of the chloroplasts which can clearly be seen in Fig. 316.

There are two ways to record a time series as the one shown in Fig. 316. A series can be recorded by defining a number of measurement cycles and activating ‘autosave’, ‘each cycle’. The function is available in any bh TCSPC FLIM module. It works well for moderate image rate and moderate numbers of pixels and time channels. A faster series, at a rate down to a few 100 ms per image, can be recorded by using the ‘continuous flow’ option of the SPC-150 in combination with the Scan Sync In mode [55, 194]. An example of a continuous flow image sequence is shown in Fig. 171, page 109.

Multi-wavelength FLIM time series can, in principle, be recorded the same way as a single-wavelength autosave time-series. However, there are more photons needed to fill 16 wavelength channels, and the amount of data to be saved is larger. That means that a multi-

wavelength FLIM series can barely be recorded faster than 1 measurement in 10 seconds. To obtain multi-wavelength images at a higher rate an 8-channel parallel TCSPC system has been designed. The system delivered high-quality FLIM data in 8 wavelength channels at a rate of 1 measurement in 5 seconds [49].

References

1. S.M. Ameer-Beg, N. Edme, M. Peter, P.R. Barber, T. Ng, B. Vojnovic, Imaging protein-protein interactions by multiphoton FLIM, Proc. SPIE, 5139, 180-189 (2003)
2. Z. Ahmed, A. C. Schüller, K. Suhling, C. Tregido, J. E. Ladbury, Extracellular point mutations in FGFR2 elicit unexpected changes in intracellular signalling. Biochem. J. 413, 37–49 (2008)
3. Z. Ahmed, R. George, C.-C. Lin, K. M. Suen, J. A. Levitt, K. Suhling, J. E. Ladbury, Direct binding of Grb2 SH3 domain to FGFR2 regulates SHP2 function. Cellular Signalling 22 23-33 (2010)
4. Z. Ahmed, C.-C. Lin, K. M. Suen, F. A. Melo, J. A. Levitt, K. Suhling, J. E. Ladbury, Grb2 controls phosphorylation of FGFR2 by inhibiting receptor kinase and Shp2 phosphatase activity. J. Cell biol. 200, 493-504 (2013)
5. K. Amari, E. Boutant, C. Hofmann, C. Schmitt-Keichinger, L. Fernandez-Calvino, P. Didier, A. Lerich, J. Mutterer, C. L. Thomas, M. Heinlein, Y. Mely, A. J. Maule, C. Ritzenthanler, A family of plasmodesmal proteins with receptor-like properties for plant viral movement proteins. PLOS Pathogens 6 e1001119-1 to -10 (2010)
6. R.M. Anderssen, K. Carlsson, A. Liljeborg, H. Brismar, Characterization of probe binding and comparison of its influence on fluorescence lifetime of two ph-sensitivy benzo[c]xantene dyes using intensity-modulated multiple-wavelength scanning technique, Analytical Biochemistry **283**, 104-110 (2000)
7. F. S. Ariola, Z. Li, C. Cornejo, R.t Bittman, A. A. Heikal, Membrane fluidity and lipid order in ternary giant unilamellar vesicles using a new bodipy-cholesterol derivative. Biophys. J. 96, 2696- 2708 (2009)
8. D. Arosio, G. Garau, F. Ricci, L. Marchetti, R. Bizzarri, R. Nifosi, F. Beltram, Spectroscopic and Structural Study of Proton and Halide Ion Cooperative Binding to GFP. Biophys. J. 93, 232-244 (2007)
9. Y. Ardeshirpour, V. Chernomordik, R. Zielinski, J. Capala, G. Griffiths, O. Vasalatiy, A. V. Smirnov, J. R. Knutson, I. Lyakhov, S. Achilefu, A. Gandjbakhche, M. Hassan, In Vivo Fluorescence Lifetime Imaging Monitors Binding of Specific Probes to Cancer Biomarkers. Plos ONE 7, e31881 (2012)
10. E. Avezov,. B.C.S. Cross, G.S. Kaminski Schierle, M. Winters, H. P. Harding, E. Pinho Melo, C. F. Kaminski, D. Ron, Lifetime imaging of a fluorescent protein sensor reveals surprising stability of ER thiol redox. J. Cell Biol. 201, 337-349 (2013)
11. B. J. Bacskai, J. Skoch, G.A. Hickey, R. Allen, B.T. Hyman, Fluorescence resonance energy transfer determinations using multiphoton fluorescence lifetime imaging microscopy to characterize amyloid-beta plaques, J. Biomed. Opt 8, 368-375 (2003)
12. B. J. Bacskai, J. Skoch, G.A. Hickey, O. Berezovska, B.T. Hyman, Multiphoton imaging in mouse models of Alzheimer's disease, Proc. SPIE, 5323, 71-76 (2004)
13. E. Baggaley, S. W. Botchway, J. W. Haycock, H. Morris, I. V. Sazanovich, J. A. G. Williams, J. A. Weinstein, Long-lived metal complexes open up microsecond lifetime imaging microscopy under multiphoton excitation: from FLIM to PLIM and beyond. Chem. Sci. 5, 879-886 (2014)
14. E. Baggaley, M. R. Gill, N. H. Green, D. Turton, I. V. Sazanovich, S. W. Botchway, C. Smythe, J. W. Haycock, J. A. Weinstein, J. A. Thomas, Dinuclear Ruthenium(II) Complexes as Two-Photon, Time-Resolved Emission Microscopy Probes for Cellular DNA. Angew. Chem. Int. Ed. Engl. 53, 3367-3371 (2014)
15. R.M. Ballew, J.N. Demas, An error analysis of the rapid lifetime determination method for the evaluation of single exponential decays, Anal. Chem. 61, 30 (1989)
16. P.R Barber, S.M Ameer-Beg, J Gilbey, L.M Carlin, M Keppler, T.C Ng, B Vojnovic, Multiphoton time-domain fluorescence lifetime imaging microscopy: practical application to protein -protein interactions using global analysis. J. R. Soc. Interface 6, S93-S105 (2009)
17. V. Bayle, L. Nussaume, and R. A. Bhat, Combination of Novel Green Fluorescent Protein Mutant TSapphire and DsRed Variant mOrange to Set Up a Versatile in Planta FRET-FLIM Assay. Plant Physiology 148, 51–60 (2008)
18. Becker & Hickl GmbH, PML-16C, 16 channel detector head for time-correlated single photon counting, user handbook, available on www.becker-hickl.com, (2006)
19. Becker & Hickl GmbH, DCC-100 detector control module, manual, available on www.becker-hickl.com
20. Becker & Hickl GmbH, SPCImage Data Analysis Software for Fluorescence Lifetime Imaging Microscopy, available on www.becker-hickl.com
21. Becker & Hickl GmbH, BDL-375SMC, BDL-405SMC, BDL-440SMC, BDL-475SMC Ultraviolet and Blue Picosecond Diode Lasers. Handbook, available on www.becker-hickl.com
22. Becker & Hickl GmbH, BDL-SMN series picosecond diode lasers. Handbook, available on www.becker-hickl.com
23. Becker & Hickl GmbH, Modular FLIM systems for Zeiss LSM 710/780/880 laser scanning microscopes. User handbook, 6th edition. (2015) Available on www.becker-hickl.com

24. Becker & Hickl GmbH, Recording the Instrument Response Function of a Multiphoton FLIM System. Application note, available on www.becker-hickl.com
25. Becker & Hickl GmbH, FLIM in the FIFO Imaging Mode: Large Images with Small TCSPC Modules. Application note, available on www.becker-hickl.com
26. Becker & Hickl GmbH, Multiphoton NDD FLIM. Application note, available on www.becker-hickl.com
27. Becker & Hickl GmbH, Non-Descanned FLIM Detection in Multiphoton Microscopes. Application note, available on www.becker-hickl.com
28. Becker & Hickl GmbH, DCS-120 Confocal FLIM System with Wideband Beamsplitter. Application note, available on www.becker-hickl.com
29. Becker & Hickl GmbH, The HPM-100-40 hybrid detector. Application note, available on www.becker-hickl.com
30. Becker & Hickl GmbH, DCS-120 Confocal Scanning FLIM System: Two-Photon Excitation with Non-Descanned Detection. Application note, available on www.becker-hickl.com
31. Becker & Hickl GmbH, Microsecond Decay FLIM: Combined Fluorescence and Phosphorescence Lifetime Imaging. Application note, available on www.becker-hickl.com
32. Becker & Hickl GmbH, Burst Analyser 2.0, for correlation analysis and single-molecule spectroscopy. Available on www.becker-hickl.com
33. Becker & Hickl GmbH, Spatially resolved recording of fluorescence-lifetime transients by line-scanning TCSPC. Application note, available on www.becker-hickl.com
34. Becker & Hickl GmbH, Megapixel FLIM with bh TCSPC Modules - The New SPCM 64-bit Software. Application note, available on www.becker-hickl.com
35. Becker & Hickl GmbH, SPC 160 Delivers Linear Intensities in High Count Rate FLIM Applications. Application note, available on www.becker-hickl.com
36. W. Becker, H. Hickl, C. Zander, K.H. Drexhage, M. Sauer, S. Siebert, J. Wolfrum, Time-resolved detection and identification of single analyte molecules in microcapillaries by time-correlated single photon counting, Rev. Sci. Instrum. 70, 1835-1841 (1999)
37. W. Becker, A. Bergmann, K. König, U. Tirlapur, Picosecond fluorescence lifetime microscopy by TCSPC imaging, Proc. SPIE 4262, 414-419 (2001)
38. W. Becker, K. Benndorf, A. Bergmann, C. Biskup, K. König, U. Tirlapur, T. Zimmer, FRET measurements by TCSPC laser scanning microscopy, Proc. SPIE 4431, 94-98 (2001)
39. W. Becker, A. Bergmann, C. Biskup, T. Zimmer, N. Klöcker, K. Benndorf, Multi-wavelength TCSPC lifetime imaging, Proc. SPIE 4620 79-84 (2002)
40. W. Becker, A. Bergmann, C. Biskup, L. Kelbauskas, T.Zimmer, N. Klöcker, K. Benndorf, High resolution TCSPC lifetime imaging, Proc. SPIE 4963, 175-184 (2003)
41. W. Becker, A. Bergmann, G. Biscotti, A. Rück, Advanced time-correlated single photon counting technique for spectroscopy and imaging in biomedical systems, Proc. SPIE 5340, 104-112 (2004)
42. W. Becker, A. Bergmann, M.A. Hink, K. König, K. Benndorf, C. Biskup, Fluorescence lifetime imaging by time-correlated single photon counting, Micr. Res. Techn. 63, 58-66 (2004)
43. W. Becker, A. Bergmann, G. Biscotti, K. Koenig, I. Riemann, L. Kelbauskas, C. Biskup, High-speed FLIM data acquisition by time-correlated single photon counting, Proc. SPIE 5323, 27-35 (2004)
44. W. Becker, A. Bergmann, E. Haustein, Z. Petrasek, P. Schwille, C. Biskup, T. Anhut, I. Riemann, K. Koenig, Fluorescence lifetime images and correlation spectra obtained by multi-dimensional TCSPC, Proc. SPIE 5700 (2005)
45. W. Becker, Adcanced time-correlated single-photon counting techniques. Springer, Berlin, Heidelberg, New York, 2005
46. W. Becker, A. Bergmann, E. Haustein, Z. Petrasek, P. Schwille, C. Biskup, L. Kelbauskas, K. Benndorf, N. Klöcker, T. Anhut, I. Riemann, K. König, Fluorescence lifetime images and correlation spectra obtained by multi-dimensional TCSPC, Micr. Res. Tech. 69, 186-195 (2006)
47. W. Becker, A. Bergmann, C. Biskup, Multi-Spectral Fluorescence Lifetime Imaging by TCSPC. Micr. Res. Tech. 70, 403-409 (2007)
48. W. Becker, A. Bergmann, Lifetime-resolved imaging in nonlinear microscopy. In: B.R. Masters, P.T.C. So, eds., Handbook of Biomedical Nonlinear Optical Microscopy.Oxford University Press 2008
49. W. Becker, B. Su, A. Bergmann, Fast-Acquisition Multispectral FLIM by Parallel TCSPC, Proc. SPIE 7183 (2009)
50. W. Becker, B. Su, K. Weisshart, O. Holub, FLIM and FCS Detection in Laser-Scanning Microscopes: Increased Efficiency by GaAsP Hybrid Detectors. Micr. Res. Tech. **74**, 804-811 (2011)
51. W. Becker, W., B. Su, A. Bergmann, K. Weisshart, O. Holub, Simultaneous Fluorescence and Phosphorescence Lifetime Imaging. Proc. SPIE **7903**, 790320 (2011)
52. W. Becker, B. Su, A. Bergmann, Spatially resolved recording of transient fluorescence lifetime effects by line-scanning TCSPC. Proc. SPIE 8226 (2012)

53. W. Becker, Fluorescence Lifetime Imaging - Techniques and Applications. J. Microsc. 247 (2) (2012)
54. W. Becker, V. Shcheslavkiy, S. Frere, I. Slutsky, Spatially Resolved Recording of Transient Fluorescence-Lifetime Effects by Line-Scanning TCSPC. Microsc. Res. Techn. 77, 216-224 (2014)
55. W. Becker, The bh TCSPC handbook. 6th edition. Becker & Hickl GmbH (2015), www.becker-hickl.com, printed copies available from bh
56. W. Becker, Introduction to Multi-Dimensional TCSPC. In W. Becker (ed.) Advanced time-correlated single photon counting applications. Springer, Berlin, Heidelberg, New York (2015)
57. W. Becker, V. Shcheslavskiy, H. Studier, TCSPC FLIM with Different Optical Scanning Techniques, in W. Becker (ed.) Advanced time-correlated single photon counting applications. Springer, Berlin, Heidelberg, New York (2015)
58. W. Becker, V. Shcheslavskiy, Fluorescence Lifetime Imaging with Near-Infrared Dyes. Photonics and Lasers in Medicine 4, 73-83 (2015)
59. J. Benesch, G. Hungerford, K. Suhling, C. Tregidgo, J. F. Mano, R. L. Reis, Fluorescence probe techniques to monitor protein adsorption-induced conformation changes on biodegradable polymers. Journal of Colloid and Interface Science 312, 193–200 195 (2007)
60. M. Y. Berezin, S. Achilefu, Fluorescence lifetime maesurement and biological imaging. Chem. Rev. 110(5), 2641-2684 (2010)
61. M.Y. Berezin, H. Lee, W. Akers, S. Achilefu, Near infrared dyes as lifetime solvatochromic probes for micropolarity measurements of biological systems. Biophys. J. 93, 2892-2899 (2007)
62. O. Berezovska, P. Ramdya, J. Skoch, M.S. Wolfe, B.J. Bacskai, B.T. Hyman, Amyloid precursor protein associates with a nicastrin-dependent docking site on the presenilin 1-γ-secretase complex in cells demonstrated by fluorescence lifetime imaging, J. Neurosci. 23, 4560-4566 (2003)
63. O. Berezovska, B.J. Bacskai, B.T. Hyman, Monitoring Proteins in Intact Cells, Science of Aging Knowledge Environment, SAGE KE 14 (2003)
64. O. Berezovska, A. Lleo, L.D. Herl, M.P. Frosch, E.A. Stern, B.J. Bacskai, B.T. Hyman, Familial Alzheimer's disease presenilin 1 mutations cause alterations in the conformation of prenesilin and interactions with amyloid precursor protein, J. Neurosci. 25, 3009-3017 (2005)
65. T. Bernas, M. Zarebski, R.R. Cook, J.W. Dobrucki, Minimizing photobleaching during confocal microscopy of fluorescent probes bound to chromatin, role of anoxia and photon flux, J. Microsc. 215, 281-296 (2004)
66. F. Bestvater, E. Spiess, G. Strobrawa, M. Hacker, T. Feurer, T. Porwolf, U. Berchner-Pfannschmidt, C. Wotzlaw, H. Acker, Two-photon fluorescence absorption and emission spectra of dyes relevant for cell imaging. J. Microsc. 208 Pt. 2, 108-115 (2002)
67. D.K. Bird, K.W. Eliceiri, C-H. Fan, J.G. White, Simultaneous two-photon spectral and lifetime fluorescence microscopy, Appl. Opt. 43, 5173-5182 (2004)
68. D.K. Bird , L. Yan , K. M. Vrotsos , K. E. Eliceiri , E. M. Vaughan. Metabolic mapping of MCF10A human breast cells via multiphoton fluorescence lifetime imaging of coenzyme NADH. Cancer Res 65:8766–8773 (2005)
69. C. Biskup, A. Böhmer, R. Pusch, L. Kelbauskas, A. Gorshkov, I. Majoul, J. Lindenau, K. Benndorf, F-D. Böhmer, Visualization of SHP-1-target interaction, J. Cell Sci. 117, 5155-5178 (2004)
70. C. Biskup, T. Zimmer, K. Benndorf, FRET between cardiac Na^+ channel subunits measured with a confocal microscope and a streak camera, Nature Biotechnology, 22(2), 220-224 (2004)
71. C. Biskup, L. Kelbauskas, T. Zimmer, K. Benndorf, A. Bergmann, W. Becker, J.P. Ruppersberg, C. Stockklausner, N. Klöcker, Interaction of PSD-95 with potassium channels visualized by fluorescence lifetime-based resonance energy transfer imaging, J. Biomed. Opt. 9, 735-759 (2004)
72. C. Biskup, L. Kelbauskas, Th. Zimmer, S. Dietrich, K. Benndorf, W. Becker, A. Bergmann, N. Klöcker, Spectrally resolved fluorescence lifetime and FRET measurements, Proc. SPIE 5700, 188-196 (2005)
73. C. Biskup, T. Zimmer, L. Kelbauskas, B. Hoffmann, N. Klöcker, W. Becker, A. Bergmann, K. Benndorf, Multi-Dimensional Fluorescence Lifetime and FRET Measurements. Micr. Res. Tech. 70, 403-409 (2007)
74. C. Biskup, B. Hoffmann, K. Benndorf, A. Rueck, Spectrally resolved lifetime imaging microscopy. In: A. Periasamy, R.M. Clegg, eds., FLIM Microscopy in Biology and Medicine. CRC Press (2009)
75. C. Biskup, Th. Gensch, Fluorescence lifetime imaging of ions in biological tissue. In: L. Marcu. P.M.W. French, D.S. Elson, (eds.), Fluorecence lifetime spectroscopy and imaging. Principles and applications in biomedical diagnostics. CRC Press, Taylor & Francis Group, Boca Raton, London, New York (2015)
76. R.A. Bhat, M. Miklis, E. Schmelzer, P. Schulze-Lefert, R. Panstruga, Recruitment and interaction dynamics of plant penetration resistance components in a plasma mebrane microdomain. PNAS 102, 3135-3140, 2005
77. F. Boal, M. Laguerre, A. Milochau, J. Lang, P. A. Scotti, A charged prominence in the linker domain of the cysteine-string protein Cspα mediates its regulated interaction with the calcium sensor synaptotagmin 9 during exocytosis. The FASEB Journal 25, 132-143 (2011)

78. J.W. Borst, M.A. Hink, A. van Hoek, A.J.W.G. Visser, Multiphoton spectroscopy in living plant cells, Proc. SPIE 4963, 231-238 (2003)
79. J. W. Borst, S. P. Laptenok, A. H. Westphal, R. Kühnemuth,H. Hornen, N. V. Visser, S. Kalinin,J. Aker, A. van Hoek, C. A. M. Seidel,A. J. W. G. Visser, Structural Changes of Yellow Cameleon Domains Observed by Quantitative FRET Analysis and Polarized Fluorescence Correlation Spectroscopy. Biophys. J. 95, 5399–5411 (2008)^
80. M. Bosch, J. Castro, T. Saneyoshi, H. Matsuno, M. Sur, Y. Hayashi, Structural and Molecular Remodeling of Dendritic Spine Substructures during Long-Term Potentiation. Neuron 82, 12059-1 to -16 (2014)
81. E. Boutant, P. Didier, A. Niehl, Y. Mely, C. Ritzenthaler, M. Heinlein, Fluorescent protein recruitment assay for demonstration and analysis of in vivo protein interactions in plant cells and its application to Tobacco mosaic virus movement protein. The Plant Journal 62, 171–177 (2010)
82. M. Brambilla, L. Spinelli, A. Pifferi, A. Torricelli, and R. Cubeddu, Time-resolved scanning system for double reflectance and transmittance fluorescence imaging of diffusive media. Rev. Sci. Instrum. 79 013103-1 to -9
83. K. Brandner, A. Sambade, E. Boutant, P. Didier, Y. Mély, C. Ritzenthaler, M. Heinlein, TMV movement protein interacts with GFP-tagged microtubule endbinding protein 1 (EB1). Plant Physiology Preview, Published on April 11, 2008, as DOI:10.1104/pp.108.117481
84. S.Y. Breusegem, In vivo investigation of protein interactions in C. Elegans by Förster resonance energy transfer microscopy, University of Illinois at Urbana-Champaign (2002)
85. H. Brismar, B. Ulfhake, Fluorescence lifetime imaging measurements in confocal microscopy of neurons labeled with multiple fluorophores, Nature Biotech. 15, 373-377 (1997)
86. I. Bugiel, K. König, H. Wabnitz, Investigations of cells by fluorescence laser scanning microscopy with subnanosecond time resolution, Lasers in the Life Sciences 3(1), 47-53 (1989)
87. N.I. Cade, G. Fruhwirth, S. J. Archibald, T. Ng, David Richards, A cellular screening assay using analysis of metal-modified fluorescence lifetime. Biophys. J. 98, 2752–2757 (2010)
88. V. Calleja, S. Ameer-Beg, B. Vojnovic, R. Woscholski, J. Downwards, B. Larijani, Monitoring conformational changes of proteins in cells by fluorescence lifetime imaging microscopy, Biochem. J. 372, 33-40 (2003)
89. J. Candelario, M.S Chachisvilis, Mechanical Stress Stimulates Conformational Changes in 5-Hydroxytryptamine Receptor 1B in Bone Cells. Cellular and Molecular Bioengineering 5, 277 (2012)
90. V. Caorsi, E. Ronzitti, G. Vicidomini, S. Krol, G. McConnell, A. Diaspro, FRET measurements on fuzzy fluorescent nanostructures. Micr. Res. Tech. 70, 452-458 (2007)
91. L. Carlini L, J.L. Nadeau, Uptake and processing of semiconductor quantum dots in living cells studied by fluorescence lifetime imaging microscopy (FLIM). Chem Commun (Camb). 49(17), 1714-6 (2013)
92. M. Chachisvilis, Y.-L. Zhang, J. A. Frangos, G protein-coupled receptors sense fluid shear stress in endothelial cells. PMAS 103, 15463-15468 (2006)
93. B. Chance, Pyridine nucleotide as an indicator of the oxygen requirements for energy-linked functions of mitochondria. Circ Res 38, I31–I38 (1976)
94. B. Chance, B. Schoener, R. Oshino, F. Itshak, Y. Nakase, Oxidation–reduction ratio studies of mitochondria in freeze-trapped samples. NADH and flavoprotein fluorescence signals J. Biol. Chem. 254, 4764–4771 (1979)
95. L.J. Charbonniere, N. Hildebrandt, Lanthanide complexes and quantum dots: A bright wedding for resonance energy transfer. Eur. J. Inorg. Chem. 2008, 3241-3251 (2008)
96. Y. Chen, J.D. Müller, P.T.C. So, E. Gratton, The Photon Counting Histogram in Fluorescence Fluctuation Spectroscopy, Biophys. J. 77, 553-567 (1999)
97. Y. Chen, A. Periasamy, Characterization of two-photon excitation fluorescence lifetime imaging microscopy for protein localization, Microsc. Res. Tech. 63, 72-80 (2004)
98. Y. Chen, A. Periasamy, Two-photon FIM-FRET microscopy for protein localization, Proc. SPIE 5323, 431-439 (2004)
99. W. Cheung, M. Gill, A. Esposito, C. F. Kaminski, N. Courousse, S. Chwetzoff, G. Trugnan, N. Keshavan, A. Lever, U. Desselberger, Rotaviruses Associate with Cellular Lipid Droplet Components To Replicate in Viroplasms, and Compounds Disrupting or Blocking Lipid Droplets Inhibit Viroplasm Formation and Viral Replication. J. Virol. 84, 6782-6798 (2010)
100. J.K. Choi, A. D'Urso, M. Trauernicht, M. Shabbir-Hussain, A. E. Holmes, M. Balaz, 3,3'-diethylthiatricarbocyanine iodide: A highly sensitive chiroptical reporter of DNA helicity and sequence. Int J Mol Sci. 12, 8052-8062 (2011)
101. D. Chorvat, A. Chorvatova, Spectrally resolved time-correlated single photon counting: a novel approach for characterization of endogenous fluorescence in isolated cardiac myocytes. Eur. Biophys. J. 36:73-83 (2006)

102. D. Chorvat, A. Mateasik, J. Kirchnerova, A. Chorvatova, Application of spectral unmixing in multi-wavelength time-resolved spectroscopy. Proc. SPIE 6771, 677105-1 to -12 (2007)
103. D. Chorvat, A. Chorvatova, Multi-wavelength fluorescence lifetime spectroscopy: a new approach to the study of endogenous fluorescence in living cells and tissues. Laser Phys. Lett. 6 175-193 (2009)
104. D.R. Cooper, K. Kudinov, P. Tyagi , C.K. Hill, S.E. Bradforth, J.L.Nadeau, Photoluminescence of cerium fluoride and cerium-doped lanthanum fluoride nanoparticles and investigation of energy transfer to photosensitizer molecules. Phys Chem Chem Phys. 16(24), 12441-53 (2014)
105. G. Cox, Optical imaging techniques in cell biology, Taylor & Francis (2007)
106. J. O. Danquah, S. Botchway, A. Jeshtadi, L. A. King, Direct Interaction of Baculovirus Capsid Proteins VP39 and EXON0 with Kinesin-1 in Insect Cells Determined by Fluorescence Resonance Energy Transfer-Fluorescence Lifetime Imaging Microscopy. J. Virol. 86, 844-853 (2012)
107. A.M. Davey, R. P. Walvick, Y. Liu, A. A. Heikal, E. D. Sheets, Membrane Order and Molecular Dynamics Associated with IgE Receptor Cross-Linking in Mast Cells. Biophys. J. 92 343-355 (2007)
108. A.M. Davey, K.M. Krise, E.D.Sheets, A.A. Heikal, Molecular perspective of antigen-mediated mast cell signaling, J. Biol.Chem. (2008)
109. R.N. Day, C.F. Booker, A. Periasamy, Characterization of an improved donor fluorescent protein for Förster resonance energy transfer microscopy. J. Biomed. Opt. 13(3), 031203-1 to -9 (2008)
110. R.N. Day, F. Schaufele, Fluorescent protein tools for studying protein dynamics in living cells: A review. J. Biomed. Opt. 13(3), 031202-1 to -6 (2008)
111. W. Denk, J.H. Strickler, W.W.W. Webb, Two-photon laser scanning fluorescence microscopy, Science 248, 73-76 (1990)
112. T. Desmettre, J.M. Devoisselle, S. Mordon, Fluorescence properties and metabolic features of indocyanine green (ICG) as related to angiography, Surv. Ophthalmol. **45**, 15-27 (2000)
113. Diaspro A. (ed.). Confocal and two-photon microscopy: Foundations, applications and advances. Wiley-Liss (2001)
114. P. Didier, G. Ulrich, Y. Mely, Raymond Ziessel, Improved push-pull-push E-Bodipy fuorophores for two-photon cell-imaging. Org. Biomol. Chem. 7, 3639-3642 (2009)
115. M. A. Digman, V. R. Caiolfa, M. Zamai, and E. Gratton, The phasor approach to fluorescence lifetime imaging analysis, Biophys J 94, L14-L16 (2008)
116. P.S. Dittrich, P. Schwille, Photobleaching and stabilization of fluorophores used for single-molecule analysis with one- and two-photon excitation, Appl. Phys. B 73, 829-837 (2001)
117. R. I. Dmitriev, A. V. Zhdanov, Y. M. Nolan, D. B. Papkovsky, Imaging of neurosphere oxygenation with phosphorescent probes. Biomaterials 34, 9307-9317 (2013)
118. R. I. Dmitriev, A. V. Kondrashina, K. Koren, I. Klimant, A. V. Zhdanov, J. M. P. Pakan, K. W. McDermott, D. B. Papkovsky, Small molecule phosphorescent probes for O2 imaging in 3D tissue models. Biomater. Sci. 2, 853-866 (2014)
119. K. Dore, S. Labrecque, C. Tardif, P. De Koninck, FRET-FLIM Investigation of PSD95-NMDA Receptor Interaction in Dendritic Spines; Control by Calpain, CaMKII and Src Family Kinase. PLOS ONE 9(11), e112170 (2014)
120. K. Douma, R.T.A. Megens, S. Reitsma, L. Prinzen, D.W. Slaaf, M.A.M.J. Van Zandvoort, Two-photon lifetime inaging of fluorescent probes in intact blood vessels: A window to sub-cellular structural information and binding status. Micr. Res. Tech. 70, 467-475 (2007)
121. D.R. Drummond, N. Carter, R.A. Cross, Multiphoton versus confocal high resolution z-sectioning of enhanced green fluorescent nanotubules: Increased multiphoton photobleaching within the focal plane can be compensated using a Pockels cell and dual widefield detectors. J. Microsc. 206, 161-169 (2001)
122. R.R. Duncan, A. Bergmann, M.A. Cousin, D.K. Apps, M.J. Shipston, Multi-dimensional time-correlated single-photon counting (TCSPC) fluorescence lifetime imaging microscopy (FLIM) to detect FRET in cells, J. Microsc. 215, 1-12 (2004)
123. C. Eggeling, S. Berger, L. Brand, J.R. Fries, J. Schaffer, A. Volkmer, C.A. Seidel, Data registration and selective single-molecule analysis using multi-parameter fluorescence detection, J. Biotechnol. 86, 163 (2001)
124. A.D. Elder, A. Domin, G.S. Kaminski Schierle, C. Lindon, J. Pines, A. Esposito, C.F. Kamiski, A quantitative protocol for dynamic measurements of protein interactions by Förster resonance energy transfer-sensitzed fluorescence emission. J. R. Soc. Interface 6, S59-S81 (2009)
125. K.W. Eliceiri, C.H. Fan, G.E. Lyons, J.G. White, Analysis of histology specimens using lifetime multiphoton microscopy, J. Biomed. Opt. 8, 376-380 (2003)
126. J.D. Ellis , D. Llères, M. Denegri , A.I. Lamond , J.F. Cáceres, Spatial mapping of splicing factor complexes involved in exon and intron definition. J. Cell Biol. 181, 921-934 (2008)

127. S. Felekyan, R. Kühnemuth, V. Kudryavtsev, C. Sandhagen, W. Becker, C.A.M. Seidel, Full correlation from picoseconds to seconds by time-resolved and time-correlated single photon detection, Rev. Sci. Instrum. 76, 083104 (2005)
128. S. Felekyan, Software package for multiparameter fluorescence spectroscopy, full correlation and multiparameter imaging. Available from www.mpc.uni-duesseldorf.de/seidel/software.htm
129. A. Ferchner, S.M. Borisov, A. V. Zhdanov, I. Klimant, D.B. Papkovsky, Intracellular O2 sensing probe based on cell-penetrating phosphorescent nanoparticles. ACS Nano 5 5499-5508 (2011)
130. J. J. Fisz, Fluorescence Polarization Spectroscopy at Combined High-Aperture Excitation and Detection: Application to One-Photon-Excitation Fluorescence Microscopy. J. Chem. Phys. A, 111, 8606-8621 (2007)
131. J.J. Fisz, Another Look at Magic-Angle-Detected Fluorescence and Emission Anisotropy Decays in Fluorescence Microscopy. J. Chem. Phys. A, 111, 12867-12870 (2007)
132. H. Fogel, S. Frere, O. Segev, S. Bharill, I. Shapira, N. Gazit, T. O'Malley, E. Slomowitz, Y. Berdichevsky, D.M. Walsh, E.Y. Isacoff, J.A. Hirsch, I. Slutsky, APP homodimers transduce an amyloid-β-mediated increase in release probability at excitatory synapses. Cell Rep. 7 1560-1576 (2014)
133. Th. Förster, Zwischenmolekulare Energiewanderung und Fluoreszenz, Ann. Phys. (Serie 6) 2, 55-75 (1948)
134. Th. Förster, Energy migration and fluorescence. Translated by Klaus Suhling. J. Biomed. Opt. 17 011002-1 to -10 (2012)
135. M.A. Fox (ed.), Photoinduced electron transfer. Elsevier, Amsterdam, Oxford, New York (1988)
136. J.H. Fox, T. Connor, M. Stiles, J. Kama, Z. Lu, K. Dorsey, G. Lieberman, E. Sapp, R.A. Cherny, M. Banks, I. Volitakis, M. DiFiglia, O. Berezovska, A.I. Bush, S.M. Hersch, Cysteine Oxidation within N-terminal Mutant Huntingtin Promotes Oligomerization and Delays Clearance of Soluble Protein. J. Biol. Chem. 286, 18320-18330 (2011)
137. S. Frere, I. Slutsky, Calcium imaging using Transient Fluorescence-Lifetime Imaging by Line-Scanning TCSPC. In: W. Becker (ed.) Advanced time-correlated single photon counting applications. Springer, Berlin, Heidelberg, New York (2015)
138. J. V. Fritz, P. Didier, J.-P. Clamme, E. Schaub, D. Muriaux, C. Cabanne, N. Morellet, S. Bouaziz, J.-L. Darlix, Y. Mély, H. de Rocquigny, Direct Vpr-Vpr Interaction in Cells monitored by two Photon Fluorescence Correlation Spectroscopy and Fluorescence Lifetime Imaging. Retrovirology 8, 87 (2008)
139. J. V. Fritz, D. Dujardin, J. Godet, P. Didier, J. De Mey, J.-L. Darli, Y. Mély, H. de Rocquigny, HIV-1 Vpr oligomerization and not that of Gag directs the interaction between Vpr and Gag. JVI (2009)
140. G. O. Fruhwirth, S. Ameer-Beg, R. Cook, T. Watson, T. Ng, F. Festy, Fluorescence lifetime endoscopy using TCSPC for the measurement of FRET in live cells. Opt. Expr. 18, 11148-11158 (2010)
141. K. Funk, A. Woitecki, C. Franjic-Würtz, Th. Gensch, F. Möhrlein, S. Frings, Modulation of chloride homeostasis by inflammatory mediators in dorsal ganglion neurons. Molecular Pain 4:32 (2008)
142. E. Gagnon, D.A. Schubert, S. Gordo, H.H. Chu, K.W. Wucherpfennig, Local Changes in lipid environment of TCR microclusters regulate membrane binding by the CD3ε cytoplasmic domain. J. Eperimental Medicine, 209, 2423 (2012)
143. S. Ganesan, S.M. Ameer-beg, T. T. C. Ng, B. Vojnovic, F.S. Wouters, A dark yellow fluorescent protein (YFP)-based Resonance Energy-Accepting Chromoprotein (REACh) for Förster resonance energy transfer with GFP. PNAS 103, 4089–4094 (2006)
144. S. Ganesan, G. Rohde, K. Eckermann, K. Sroka, M.K.E. Schaefer, C.P, Dohm, P. Kermer, G. Haase, F. Wouters, M. Bähr, J.H, Weishaupt, Mutant SOD1 detoxification mechanisms in intact single cells. Cell Death Differ. 15(2) (2008), 312-321
145. I. Gannot, I. Ron, F. Hekmat, V. Chernomordik, A. Ganjbakhche, Functional optical detection based on pH dependent fluorescence lifetime, Lasers in Surgery and Medicine **35**, 342-348 (2004)
146. D. I. Garcia, P. Lanigan, M. Webb, T. G. West, J. Requejo-Isidro, E. Auksorius, C. Dunsby, M. Neil, P. French, M. A. Ferenczi, Fluorescence Lifetime Imaging to Detect Actomyosin States in Mammalian Muscle Sarcomeres. Biophys. J. 93, 2091-2101 (2007)
147. C.D. Geddes, H. Cao, I. Gryczynski, J. Fang, J.R. Lakowicz, Metal-enhanced fluorescence (MEF) due to silver colloids on a planar surface: Potential applications of indocyanine green to in vivo imaging, J. Phys. Chem. A 107, 3443-3449 (2003)
148. Th. Gensch, V. Untiet, A. Franzen, P. Kovermann, C. Fahlke, Determination of Intracellular Chloride Concentrations by Fluorescence Lifetime Imaging. In: W. Becker (ed.) Advanced time-correlated single photon counting applications. Springer, Berlin, Heidelberg, New York (2015)
149. R. George, H.-L. Chan, Z. Ahmed, K. M. Suen, C. N. Stevens, J. A. Levitt, K. Suhling, J. Timms, J. E. Ladbury, A complex of Shc and Ran-GTPase localises to the cell nucleus. Cell. Mol. Life Sci. 66 711 – 720 (2009)

150. M. Georgin, L. Carlini, D. Cooper, S.E. Bradforth, J.L. Nadeau, Differential effects of β-mercaptoethanol on CdSe/ZnS and InP/ZnS quantum dots. Phys Chem Chem Phys. 15(25), 10418-28 (2013)
151. H.C. Gerritsen, R. Sanders, A. Draaijer, Y.K. Levine, Fluorescence lifetime imaging of oxygen in cells, J. Fluoresc. 7, 11-16 (1997)
152. H.C. Gerritsen, M.A.H. Asselbergs, A.V. Agronskaia, W.G.J.H.M. van Sark, Fluorescence lifetime imaging in scanning microscopes: acquisition speed, photon economy and lifetime resolution, J. Microsc. 206, 218-224 (2002)
153. V. Ghukasyan, Y.-Y. Hsu, S.-H. Kung, F.-J. Kao, Application of fluorescence resonance energy transfer resolved by fluorescence lifetime imaging microscopy for the detection of enterovirus 71 infection in cells, J. Biomed. Opt. 12, 024016-1 to -8 (2007)
154. V. Ghukassian, F.-J. Kao, Monitoring cellular metabolism with fluorescence lifetime of reduced nicotinamide adenine dinucleotide. J. Phys. Chem. C, 113, 11532-11540 (2009)
155. V. Ghukasyan, C.C. Hsu, C.R. Liu, F.J. Kao, T.H. Cheng, Fluorescence lifetime dynamics of enhanced green fluorescent protein aggregates with expanded polyglutamine. J. Biomed. Opt. 15(1) 016008-1 to -11 (2010)
156. D. Gilbert, C. Franjic-Würtz, K. Funk, T. Gensch, S. Frings, F. Möhrlen, Differential maturation of chloride homeostasis in primary afferent neurons of the somatosensory system. Int. J. Devl. Neuroscience 25, 479-489 (2007)
157. M. Göppert-Mayer, Über Elementarakte mit zwei Quantensprüngen, Ann. Phys. 9, 273-294 (1931)
158. G.W. Gordon, G. Berry, X.H. Liang, B. Levine, B. Herman, Quantitative Fluorescence Resonance Energy Transfer Measurements Using Fluorescence Microscopy. Biophys. J. 74, 2702-2713 (1998)
159. P. Gorlovoy, S. Larionov, T. T. H. Pham, H. Neumann, Accumulation of tau induced in neurites by microglial proinflammatory mediators. The FASEB Journal 23, 2502-2513 (2009)
160. Govindjee, Sixty-three Years Since Kautsky: Chlorophyll α Fluorescence, Aust. J. Plant Physiol. **22**, 131-160 (1995)
161. Govindjee, M.J. Seufferheld, Non-photochemical quenching of chlorophyll α Fluorescence: Early history and characterization of two xanthophyll-cycle mutants of Chlamydomonas Reinhardtii, Funct. Plant Biol. **29**, 1141-1155 (2002)
162. V. J. Greiner, V. Shvadchak, J. Fritz, Y. Arntz, P. Didier, B. Frisch, C. Boudier, Y. Mély, H. de Rocquigny, Characterization of the mechanisms of HIV-1 Vpr(52e96) internalization in cells. Biochimie 93 1647-1658 (2011)
163. C. Guardia-Laguarta, M. Coma, M. Pera, J. Clarimon, L. Sereno, J.M. Agullo, L. Molina-Porcel, E. Gallordo, A. Deng, O. Berezovska, B. Hyman, R. Blesa, T. Gomez-Isla, A. Lleo, Mild cholesterol depletion reduces amyloid-β production by impairing APP trafficking to the cell surface. J. Neurochem. 110, 220-230 (2009)
164. Q. Guo , J. E. Jureller, J. T. Warren, E. Solomaha, J. Florian, W.-J. Tang, Protein-Protein Docking and Analysis Reveal That Two Homologous Bacterial Adenylyl Cyclase Toxins Interact with Calmodulin Differently. JBC 283, 23836-23845 (2008)
165. A. Habenicht, J. Hjelm, E. Mukhtar, F. Bergström, L.B-A. Johansson, Two-photon excitation and time-resolved fluorescence: I. The proper response function for analysing single-photon counting experiments, Chem. Phys. Lett. 345, 367-375 (2002)
166. A. Hayek, A. Grichine, T. Huault, C. Ricard, F. Bolze, B. van der Sanden, J.-C. Vial, Y. Mely, A. Duperray, P. L. Balldeck, J.-F. Nicoud, Cell-Permeant Cytoplasmic Blue Fluorophores Optimized for In Vivo Two-Photon Microscopy With Low-Power Excitation. Micr. Res. Techn. 70 880-885 (2007)
167. C. K. Haluska, A. P. Schröder, P. Didier, D. Heissler, G. Duportail, Y. Mely, C. M. Marques, Combining Fluorescence Lifetime and Polarization Microscopy to Discriminate Phase Separated Domains in Giant Unilamellar Vesicles. Biophys. J. 95, 5737-5747 (2008)
168. Hamamatsu Photonics K.K., R3809U-50 series Microchannel plate photomultiplier tube (MCP-PMTs) (2001)
169. Hamamatsu Photonics K.K., H7422 series Metal package PMT with cooler - photosensor modules (2003)
170. K.M. Hanson, M.J. Behne, N.P. Barry, T.M. Mauro, E. Gratton, Two-photon fluorescence imaging of the skin stratum corneum pH gradient, Biophys. J. 83, 1682-1690 (2002)
171. G. T. Hanson, R. Aggeler, D. Oglesbee, M. Cannon, R. A. Capaldi,R. Y. Tsien, S. J. Remington, Investigating Mitochondrial Redox Potential with Redox-sensitiveGreen Fluorescent Protein Indicators. J. Biol. Chem., 279, 13044-13053 (2004)
172. M. E. Haque, L. L. Spremulli, C. J. Fecko, Identification of Protein-Protein and Protein-Ribosome Interacting Regions of the C-terminal Tail of Human Mitochondrial Inner Membrane Protein Oxa1L. J. Biol. Chem. 285, 34991-34998 (2010)
173. R.P. Haugland, Handbook of fluorescent probes and research chemicals, 7th Ed. Molecular Probes, Inc. (1999)

174. S.W. Hell, M. Booth, S. Wilms, Two-photon near- and far-field fluorescence microscopy with continuous-wave excitation, Opt. Lett. **23**, 1238-1240 (1998)
175. T. Hellerer, New ultrachrome light source for microscopy, Laser+Photonics 4, 36-38, 2009
176. L. Herl, A. V. Thomas, C. M. Lill, M. Banks, A. Deng, P. B. Jones, R. Spoelgen, B. T. Hyman, O. Berezovska, Mutations in amyloid precursor protein affect its interactions with presenilin/γ-secretase. Molecular and Cellular Neuroscience 41, 166–174 (2009)
177. B. Herman, G. Gordon, N. Mahajan, V. Centonze, Measurement of fluorescence resonance energy transfer in the optical microscpe. In A. Periasamy (ed.), Methods of cellular imaging, Oxford University Press (2001)
178. B. Hoffmann, Thomas Zimmer, N. Klöcker, L. Kelbauskas, K. König, K. Benndorf, C. Biskup, Prolonged irradiation of enhanced cyan fluorescent protein or Cerulean can invalidate Förster resonance energy transfer measurements. J. Biomed. Opt. 13(3), 031250-1 to -9 (2008)
179. A. Hopt, E. Neher, Highly nonlinear Photodamage in two-photon fluorescence microscopy, Biophys. J. 80, 2029-2036 (2002)
180. N. A. Hosny, G. Mohamedi, P. Rademeyer, J. Owen, Y. Wu, M. X. Tang, R. J. Eckersley, E. Stride, and M. K. Kuimova, Mapping microbubble viscosity using fluorescence lifetime imaging of molecular rotors. Proc Natl Acad Sci U S A 110, 9225-9230 (2013)
181. C. Huang, P.J. Butler, S. Tong, H.S. Muddana, G. Bao, S. Zhang, Substrate stiffness regulates cellular uptake of nanoparticles. Nano Lett. 13, 1611-1615, (2013)
182. M.K.Y. Hughes, S. Ameer-Beg, M. Peter, T. Ng, Use of acceptor fluorescence for determining FRET lifetimes, Proc. SPIE 5139, 88-96 (2003)
183. B. Ilien, N. Glasser, J.-P. Clamme, P. Didier, E. Piemont, R. Chinnappan, S. B. Daval, J.-L. Galzi, Y. Mely, Pirenzepine Promotes the Dimerization of Muscarinic M1 Receptors through a Three-step Binding Process. J. Biol. Chem. 284(29) 19533–19543, (2009)
184. M. M. Janas, B. Wang, A. S. Harris, M. Aguiar, J. M. Shaffer, Y. V. B. K. Subrahmanyam, M. A. Behlke, K. W. Wucherpfennig, S. P. Gygi, E. Gagnon, and C. D. Novina, Alternative RISC assembly: binding and repression of microRNA-mRNA duplexes by human Ago proteins. RNA N. Y. N, 18, no. 11, 2041–2055 (2012)
185. J. Jenkins, R. I. Dmitriev, D. B. Papkovsky, Imaging Cell and Tissue O_2 by TCSPC-PLIM. In: W. Becker (ed.) Advanced time-correlated single photon counting applications. Springer, Berlin, Heidelberg, New York (2015)
186. A. Jeshtadi, P. Burgos, C. D. Stubbs, A. W. Parker, L. A. King, M. A. Skinner, S. W. Botchway, Interaction of Poxvirus Intracellular Mature Virion Proteins with the TPR Domain of Kinesin Light Chain in Live Infected Cells Revealed by Two-Photon-Induced Fluorescence Resonance Energy Transfer Fluorescence Lifetime Imaging Microscopy. J. Virol. 84, 12886-12894 (2010)
187. Y. Jiang, L. A. Borrelli, Y. Kanaoka, B. J. Bacskai, J. A. Boyce, CysLT2 receptors interact with CysLT1 receptors and down-modulate cysteinyl leukotriene–dependent mitogenic responses of mast cells. Blood 110, 3263-3270 (2007)
188. P.B. Jones, A. Rozkalne, M. Meyer-Luehmann, T.L. Spires-Jones, A. Makarova, A.T.N. Kumar, O. Berezovska, B.B. Bacskai, B. Hyman, Two postprocessing techniques for the elimination of background autofluorescence for fluorescence lifetime imaging microscopy. J. Biomed. Opt. 13(1) 014008-1 to -8 (2008)
189. P. B. Jones, K.W. Adams, A. Rozkalne, T.L. Spires-Jones, T.T. Hshieh, T. Hashimoto1, C.A. F. von Armin, M. Mielke, B.J. Bacskai, B.T. Hyman, Apolipoprotein E: Isoform Specific Differences in Tertiary Structure and Interaction with Amyloid-b in Human Alzheimer Brain. PLoS One 6, e14586 (2011)
190. V. Jyothikumar, Y. Sun, A. Periasamy, Investigation of tyrptopahn-NADH in live human cells using 3-photon fluorescence lifetime imaging. J. Biomed. Opt. 18(6), 060501 (2013)
191. H. Kaneko, I. Putzier, S. Frings, U. B. Kaupp, and Th. Gensch, Chloride Accumulation in Mammalian Olfactory Sensory Neurons, J. Neurosci., 24(36) 7931-7938 (2004)
192. S. R. Kantelhardt, J. Leppert, J. Krajewski, N. Petkus, E. Reusche, V. M. Tronnier, G. Hüttmann, A. Giese, Imaging of brain and brain tumor specimens by time-resolved multiphoton excitation microscopy ex vivo. Neuro-Onkology April 2007, 103-112
193. D. Kapsokalyvas, P.M.H. Schiffers, N. Maij, D.P. Suylen, T.M. Hackeng, M.A.M.J. van Zandvoort, J.G.R. DeMey, Imaging evidence for endothelin ETA/ETB receptor heterodimers in isolated rat mesenteric resistance arteries. Life Sciences 111, 36-41 (2014)
194. V. Katsoulidou, A. Bergmann, W. Becker, How fast can TCSPC FLIM be made? Proc. SPIE 6771, 67710B-1 to 67710B-7
195. H. Kautsky, A. Hirsch, Neue Versuche zur Kohlensäureassimilation, Naturwissenschaften **19**, 964 (1931)

196. L. Kelbauskas, W. Dietel, Internalization of aggregated photosensitizers by tumor cells: Subcellular time-resolved fluorescence spectroscopy on derivates of pyropheophorbide-a ethers and chlorin e6 under femtosecond one- and two-photon excitation, Photochem. Photobiol. 76, 686-694 (2002)
197. T. Kelleher, G. Fruhwirth, G. Patel, E. Ofo, F. Festy, P.R. Barber, S.M. Ameer-Beg, B. Vojnovic, C. Gillett, A. Coolen, G. Kéri, P.A. Ellis, T. Ng, The potential of optical proteomic technologies to individualize prognosis and guide rational treatment for cancer patients. Targ. Oncol. 4, 235–252 (2009)
198. D. Kepshire, N. Mincu, M. Hutchins, J. Gruber, H. Dehghani, J. Hypnarowski, F. Leblond, M. Khayat, B. W. Pogue, A microcomputed tomography guided fluorescence tomography system for small animal molecular imaging. Rev. Sci. Instrum. 80, 043701-1 to -10 (2009)
199. D. J. Killock, M. Parsons, M. Zarrouk, S. M. Ameer-Beg, A. J. Ridley, D. O. Haskard, M. Zvelebil, A. Ivetic, In Vitro and in Vivo Characterization of Molecular Interactions between Calmodulin Ezrin/Radixin/Moesin, and L-selectin. Journal of Biological Chemisty, JBC, 284 8833-8845 (2009)
200. K. Kirchberg, T.-Y Kim, M. Möller, D. Skegro, G. D. Raju, j. Granzin, G. Büldt, R. Schlesinger, U. Alexiev, Conformational dynamics of helix 8 in the GPCR rhodopsin arrestin activation in the desnsitization process. PNAS 108, 18690-18695 (2011)
201. J. Klucken, T. F. Outeiro, P. Nguyen, P. J. McLean, B. T. Hyman, Detection of novel intracellular-synuclein oligomeric species by fluorescence lifetime imaging. FASEB J. 20, 2050-2057 (2006)
202. J-P. Knemeyer, N. Marmé, M. Sauer, Probes for detection of specific DNA sequences at the single-molecule level, Anal. Chem. 72, 3717-3724 (2002)
203. M. Köllner, J. Wolfrum, How many photons are necessary for fluorescence-lifetime measurements?, Phys. Chem. Lett. 200, 199-204 (1992)
204. M. J. Koehler, K. König, P. Elsner, R. Bückle, M. Kaatz, In vivo assessment of human skin aging by multiphoton laser scanning tomography, Opt. Lett. 31, 2879-2881 (2006)
205. K. König, P.T.C. So, W.W. Mantulin, B.J. Tromberg, E. Gratton, Two-Photon excited lifetime imaging of autofluorescence in cells during UVA and NIR photostress, J. Microsc. **183**, 197-204 (1996)
206. K. König, Multiphoton microscopy in life sciences, J. Microsc. 200, 83-104 (2000)
207. K. König, Laser tweezers and multiphoton microscopes on life science, Histochem. Cell Biol. 114, 79-92 (2000)
208. K. König, Cellular Response to Laser Radiation in Fluorescence Microscopes, in A. Periasamy, Methods in Cellular Imaging, Oxford University Press, 236-254 (2001)
209. K. König, U. Wollina, I. Riemann, C. Peuckert, K-J. Halbhuber, H. Konrad, P. Fischer, V. Fuenfstueck, T.W. Fischer, P. Elsner, Optical tomography of human skin with subcellular resolution and picosecond time resolution using intense near infrared femtosecond laser pulses, Proc. SPIE 4620, 191-202 (2002)
210. K. König, I. Riemann, High-resolution multiphoton tomography of human skin with subcellular spatial resolution and picosecond time resolution, J. Biom. Opt. 8, 432-439 (2003)
211. K. König, I. Riemann, G. Ehrlich, V. Ulrich, P. Fischer, Multiphoton FLIM and spectral imaging of cells and tissue, Proc. SPIE 5323, 240-251 (2004)
212. K. Koenig, Clinical multiphoton tomography. J. Biophoton. 1, 13–23 (2008)
213. K. König, Multiphoton-induced cell damage. In: B.R. Masters, P.T.C. So, eds., Handbook of Biomedical Nonlinear Optical Microscopy.Oxford University Press 2008
214. K. König, A. Uchugonova, Multiphoton Fluorescence Lifetime Imaging at the Dawn of Clinical Application. In: A. Periasamy, R.M. Clegg, eds., FLIM Microscopy in Biology and Medicine. CRC Press 2009
215. S. V. Koushik, H. Chen, C. Thaler, H. L. Puhl, and S. S. Vogel, Cerulean, Venus, and VenusY67C FRET Reference Standards. Biophys J.: Biophysical Letters L99-L101 (2006)
216. S.V. Koushik, S.S. Vogel, Energy migration alters the fluorescence lifetime of Cerulean: implications for fluorescence lifetime imaging Forster resonance energy transfer measurements. J. Biomed. Opt. 13(3), 031204-1 to -9 (2008)
217. S.V. Koushik, P.S. Blank, S.S. Vogel, Anomalous Surplus Energy Transfer Observed with Multiple FRET Acceptors. www.plosone.org, PLOS ONE 4 Issue 11, e8031 (2009)
218. M. Krieg, A.R. Dunn, and M.B. Goodman, Mechanical control of the sense of touch by β spectrin. Nat Cell Biol. 16(3), 224–233 (2014)
219. K.V. Kuchibhotla, C.R. Lattarulo, B. Hyman, B. J. Bacskai, Synchronous hyperactivity and intercellular calcium waves in astrocytes in Alzheimer mice. Science 323, 1211-1215
220. M. K. Kuimova, G. Yahioglu, J. A. Levitt, K. Suhling, Molecular Rotor Measures Viscosity of Live Cells via Fluorescence Lifetime Imaging. J. Am. Chem. Soc. 130, 6672–6673 (2008)
221. K.T. Kumfer, S.J. Cook, J.M.Squirrell, K.W. Eliceiri, N. Peel, K.F. O'Connel, J.G. White, CGEF-1 and CHIN-1 regulate CDC-42 activity during asymmetric division in the Caenorhabditis elegans embryo. Molecular Biology of the Cell 21, 266-277 (2010)

222. M. Kwaaitaal, N.F. Keinath, Simone Pajonk, C. Biskup, R. Panstruga, Combined Bimolecular Fluorescence Complementation and Förster Resonance Energy Transfer Reveals Ternary SNARE Complex Formation in Living Plant Cells. Plant Physiology 152, 1135-1147 (2010)
223. J.R. Lakowicz, I. Gryczynski, W. Wiczk, J. Kusba, M. Johnson, Correction for incomplete labeling in the measurement of distance distributions by frequency-domain fluorometry, Anal. Biochem. 195, 243-254 (1991)
224. J.R. Lakowicz, H. Szmacinski, K. Nowaczyk, M.L. Johnson, Fluorescence lifetime imaging of free and protein-bound NADH, PNAS 89, 1271-1275 (1992)
225. Lakowicz J.R., Szmacinski H., Johnson M.L., Calcium imaging using fluorescence lifetimes an long-wavelength probes. J. Fluoresc. 2, 47-62 (1992)
226. J.R. Lakowicz, Principles of Fluorescence Spectroscopy, 3rd edn., Springer (2006)
227. E. Lapointe, J. Pichette, and Y. Berube-Lauziere, A multi-view time-domain non-contact diffuse optical tomography scanner with dual wavelength detection for intrinsic and fluorescence small animal imaging. Rev. Sci. Instrum. 83, 063703-1 to -14 (2012)
228. R.A. La Rue, K.A. Costello, G.A. Davis, J.P. Edgecumbe, V.W. Aebi, Photon Counting III-V Hybrid Photomultipliers Using Transmission Mode Photocathodes. IEEE Transactions on Electron Devices 44, 672-678 (1997)
229. A. Y. Lebedev, A. V. Cheprakov, S. Sakadzic, D. A. Boas, D. F. Wilson, Sergei A. Vinogradov, Dendritic Phosphorescent Probes for Oxygen Imaging in Biological Systems. Applied Materials & Interfaces 1, 1292-1304 (2009)
230. J. Leppert, J. Krajewski, S.R. Kantelhardt, S. Schlaffer, N. Petkus, E. Reusche, G. Hüttmann, A. Giese, Multiphoton excitation of autofluorescence for microscopy of glioma tissue. Neurosurgery 58, 759-767 (2006)
231. R. W. K. Leung, S.-C. A. Yeh, Q. Fang, Effects of incomplete decay in fluorescence lifetime estimation. Biomed. Opt. Expr. 2, 2517-2531
232. J. A. Levitt, M. K. Kuimova, G. Yahioglu, P.-H. Chung, K. Suhling, D. Phillips, Membrane-Bound Molecular Rotors Measure Viscosity in Live Cells via Fluorescence Lifetime Imaging. J. Phys. Chem. C 2009, 113, 11634–11642
233. A. Liebert, H. Wabnitz, J. Steinbrink, M. Möller, R. Macdonald, H. Rinneberg, A. Villringer, H. Obrig, Bed-side assessment of cerebral perfusion in stroke patients based on optical monitoring of a dye bolus by time-resolved diffuse reflectance, NeuroImage **24**, 426-435 (2005)
234. Q. Li, S. Seeger, Label-free detection of protein interactions using deep UV fluorescence lifetime microscopy. Anl. Biochem. 367 104-110 (2007)
235. L.L. Lin, J. E. Grice, M.K. Butler, A.V. Zvyagin, W. Becker, T. A. Robertson, H.P. Soyer, M. S. Roberts, T.W. Prow, Time-correlated single photon counting for Simultaneous monitoring of zinc oxide nanoparticles and NAD(P)H in intact and barrier-disrupted volunteer skin. Pharm Res. DOI 10.1007/s11095-011-0515-5 (2011)
236. Y. Liu, S. Walter, M. Stagi, D. Cherny, M. Letiembre. W. Schulz-Schaeffer, H. Heine, B. Penke, H. Neumann, K. Fassbender, LPS receptor (CD 4): a receptor for phagocytosis of Alzheimer's amyliod peptide. Brain 28, 778-789 (2005)
237. A. Lleo, O. Berezovska, L. Herl, S. Raju, A. Deng, B.J. Bacskai, M.P. Frosch, M. Irizarry, B.T. Hyman, Nonsteroidal anti-inflammatory drugs lower Aβ42 and change presenilin 1 conformation, Nature Medicine 10, 1065-1066 (2004)
238. D. Lleres, S. Swift, A. I. Lamond, Detecting Protein-Protein Interactions In Vivo with FRET using Multiphoton Fluorescence Lifetime Imaging Microscopy (FLIM). Curr. Protoc. Cytom. 42, 12.10.1-12.10.19 (2007)
239. D. Lleres, J. James, S. Swift, D.G. Norman, A. I. Lamond, Quantitative analysis of chromatin compaction in living cells using FLIM-FRET. J. Cell Biol. 187, 481-191 (2009)
240. K. Makrogianneli, L. M. Carlin, M. D. Keppler, D. R. Matthews, E. Ofo, A. Coolen, S. M. Ameer-Beg, P. R. Barber, B. Vojnovic, T. Ng, Integrating Receptor Signal Inputs That Influence Small Rho GTPase Activation Dynamics at the Immunological Synapse. Mol. Cell. Biol. 29, 2997–3006 (2009)
241. J. Malicka, I. Gryczynski, C.D. Geddes, J.R. Lakowicz, Metal-enhanced emission from indocyanine green: a new approach to in vivo imaging, J. Biomed. Opt. 8, 472-478 (2003)
242. A. K. Mandal, J. Skoch, B. J. Bacskai, B. T. Hyman, P. Christmas, D. Miller, T. D. Yamin, S. Xu, D. Wisniewski, J. F. Evans, and R. J. Soberman, The membrane organization of leukotriene synthesis. PNAS 101, 6587-6592 (2004)
243. M. L. Martin-Fernandez, Human epidermal growth factor receptor (HER1) aligned on the plasma membrane adopts key features of *Drosophila* EGFR asymmetry, Biochemical Society Transactions 40, 184–188, (2012)

244. B.R. Masters, P.T.C. So, eds., Handbook of Biomedical Nonlinear Optical Microscopy.Oxford University Press 2008
245. K. Maxwell, G.N. Johnson, Chlorophyll fluorescence - a practical guide, Journal of Experimental Botany **51**, 659-668 (2000)
246. D. X. Medina, A. Caccamo, S. Oddo, Methylene blue reduces Aβ levels and rescues early cognitive deficit by increasing proteasome activity. Brain Pathol. 21, 140–149 (2011)
247. C.N. Medine, A. McDonald, A, Bergmann, R. Duncan, Time-correlated single photon counting FLIM: Some considerations for Physiologists. Micr. Res. Tech. 70, 421-425 (2007)
248. I.L. Medintz, T. Pons, K. Susumu, K. Boeneman, A.M. Dennis, D. Farrel, J.R.Deschamps, J.S. Melinger, G. Bao, H. Mattoussi, Resonance energy trensfer between luminescent quantum dots and diverse fluorescent protein acceptors. J. Phy. Chem. C 113, 18552-18560 (2009)
249. I. L. Medintz, M. H. Stewart, S. A. Trammell, K. Susumu, J. B. Delehanty, B. C. Mei, J. S. Melinger, J. B. Blanco-Canosa, P. E. Dawson, H. Mattoussi, Quantum-dot/dopamine bioconjugates functionas redox coupled assemblies for in vitro and intracellular pH sensing. Natrure Materials, 9, 676-684 (2010)
250. P. Mergenthaler, A. Kahl, A. Kamitz, V. van Laak, K. Stohlmann, Susanne Thomsen, H. Klawitter, I. Przesdzing, Lars Neeb, D Freyer, J Priller, T J. Collins, D. Megow, U. Dirnagl, D. W. Andrews, A. Meisel, Mitochondrial hexokinase II (HKII) and phosphoprotein enriched in astrocytes (PEA15) form a molecular switch governing cellular fate depending on the metabolic state. PNAS 109, 1518-1523
251. F. Mies, C. Spriet, L. Heliot, S. Sariban-Sohraby, Epithelial Na+ channel stimulation by n-3 fatty acids requires proximity to a membrane-bound A-kinase-anchoring protein complexed with protein kinase A and phosphodiestrase. J. Biol. Chem. 282 18339-18347 (2007)
252. M. Minsky, US Patent 3013467, (1957)
253. M. Minsky, Memoir on inventing the confocal microscope, Scanning 10, 128-138 (1988)
254. A. Minta, J.P.Y. Kao, R.Y. Tsien, Fluorescent indicators for cytosolic calcium based on rhodamine and fluorescein chromophores, J. Biol. Chem. 264, 8171-8178 (1989)
255. S. Miserey-Lenkei, F. Waharte, A. Boulet, M.-H. Cuif, D. Tenza, A. El Marjou, G. Raposo, J. Salamero, L. Heliot, B. Goud, S. Monier, Rab6-interacting protein 1 links Rab6 and Rab 11 function. Traffic 8, 1385-1403 (2007)
256. Thomas T. Morgan, Hari S. Muddana, Erhan I. Altnoglu, Sarah M. Rouse, Amra Tabakovic, Tristan Tabouillot, Timothy J. Russin, Sriram S. Shanmugavelandy, Peter J. Butler, Peter C. Eklund, Jong K. Yun, Mark Kester, James H. Adair, Encapsulation of Organic Molecules in Calcium Phosphate Nanocomposite Particles for Intracellular Imaging and Drug Delivery. Nano Lett. 8, 4108-4115 (2008)
257. P.E. Morton, T.C. Ng, S.A. Roberts, B. Vojnovic, S.M. Ameer-Beg, Time resolved multiphoton imaging of the interaction between the PKC and NFkB signalling pathways, Proc. SPIE 5139, 216-222 (2003)
258. Hari S. Muddana, Thomas T. Morgan, James H. Adair, and Peter J. Butler, Photophysics of Cy3-Encapsulated Calcium Phosphate Nanoparticles. Nano Lett. (2009)
259. J.D. Müller, Y. Chen, E. Gratton, Resolving Heterogeneity on the single molecular level with the photon-counting histogram, Biophys. J. 78, 474-586 (2000)
260. I. Mueller-Harvey, W. Feucht, J. Polster, L. Trnkova, P. Burgos, A.W. Parker, S.W. Botchway, Two-photon excitation with pico-seond fluorescence lifetime imaging to detect nuclear association of flavanols. Analytica Chimica Acta 719, 68-75 (2012)
261. H. Murakoshi, S-J. Lee, R. Yasuda, Highly sensitive and quantitative FRET–FLIM imaging in single dendritic spines using improved non-radiative YFP. Brain Cell Biol. 36, 31-42 (2008)
262. L. Munsie, N. Caron, R. S. Atwal, I. Marsden, E. J. Wild, J. R. Bamburg, S. J. Tabrizi, R. Truant, Mutant huntingtin causes defective actin remodeling during stress: defining a new role for transglutaminase 2 in neurodegenerative disease. Human Molecular Genetics, 2011, Vol. 20, No. 10 1937–1951
263. T.A. Nguyen, P. Sarkar, J.V. Veetil, S.V. Koushik, S.S. Vogel, Fluorescence Polarization and Fluctuation Analysis Monitors Subunit Proximity, Stoichiometry, and Protein Complex Hydrodynamics. PLoS ONE 7, e38209-1 to -13 (2012)
264. A. C. Nyborg, L. Herl, O. Berezovska, A. V Thomas, T. B. Ladd, K. Jansen, B. T. Hyman, T. E. Golde, Signal peptide peptidase (SPP) dimer formation as assessed by fluorescence lifetime imaging microscopy (FLIM) in intact cells. Mol. Neurodegener. 1:16 (2006)
265. A. Oliveira, R. Yasuda, An improved Ras Sensor for highly sensitive and quantitative FRET-FLIM inaing. PLOS ONE 8 e52874 (2013)
266. D.V. O'Connor, D. Phillips, Time-correlated single photon counting, Academic Press, London (1984)
267. A. Osterrieder, C.M. Carvalho1, M Latijnhouwers, J. N. Johansen1, C. Stubbs, S. Botchway, C. Hawes, Fluorescence Lifetime Imaging of Interactions between Golgi Tethering Factors and Small GTPases in Plants. Traffic 10, 1-13 (2009)

268. Z. J. Palmer, R. R. Duncan, J. R. Johnson, L.-Y. Lian, L. V. Mello, D. Booth., Jeff W. Barclay, M. E. Graham, R. D. Burgoyne, I. A. Prior and Alan Morgan, S-nitrosylation of syntaxin 1 at Cys145 is a regulatory switch controlling Munc18-1 binding. Biochem. J. 413479-491 (2008)
269. D. Papkovsky, A. V. Zhdanov, A. Fercher, R. I. Dmitriev, and J. Hynes, Phosphorescent oxygen-sensitive probes (Springer, 2012)
270. D. B. Papkovsky, and R. I. Dmitriev, Biological detection by optical oxygen sensing, Chem Soc Rev 42, 8700-8732 (2013)
271. G.H. Patterson, D.W. Piston, Photobleaching in two-photon excitation microscopy, Biophys. J. 78, 2159-2162 (2000)
272. R.J. Paul, H. Schneckenburger, Oxygen concentration and the oxidation-reduction state of yeast: Determination of free/bound NADH and flavins by time-resolved spectroscopy, Naturwissenschaften 83, 32-35 (1996)
273. J. Pawley (ed.), Handbook of biological confocal microscopy, 2nd edn., Plenum Press, New York (1995)
274. S. Pelet, M.J.R. Previte, P.T.C. So, Comparing the quantification of Förster resonance energy transfer measurement accuracies based on intensity, spectral, and lifetime imaging. J. Biomed. Opt. 11 034017-1 to -11 (1006)
275. I. D. Peltan, A.V. Thomas, I. Mikhailenko, D. K. Strickland, B. T. Hyman, C.A.F. von Arnim, Fluorescence lifetime imaging microscopy (FLIM) detects stimulus-dependent phospholylation of the low density lipoprotein receptor-related protein (LRP) in primary neurons. Biochem. Biophys. Res. Commun. 349, 24-30 (2006)
276. A. Periasamy, Methods in Cellular Imaging. Oxford University Press, Oxford New York (2001)
277. A. Periasamy, R.M. Clegg, eds., FLIM Microscopy in Biology and Medicine. CRC Press 2009
278. A. Periasamy, N. Mazumder, Y. Sun, K. G. Christopher, R. N. Day, FRET Microscopy: Basics, Issues and Advantages of FLIM-FRET Imaging. In: W. Becker (ed.) Advanced time-correlated single photon counting applications. Springer, Berlin, Heidelberg, New York (2015)
279. M. B. M. Pereira, A. M. Santos, D. C. Goncalves, A. C. Cardoso, S. R. Consonni, Fabio C. Gozzo, P. S. Oliveira, A. H. M. Pereira, A. R. Figueiredo, A. O. Tiroli-Cepeda, C. H. I. Ramos, A A. de Thomaz, Carlos L. Cesar, K. G. Franchini, αB-crystallin interacts with and prevents stress-activated proteolysis of focal adhesion kinase by calpain in cardiomyocytes. Nature Communications, 5, 5159 (2014)
280. M. Peter, S.M. Ameer-Beg, Imaging molecular interactions by multiphoton FLIM, Biology of the Cell 96, 231-236 (2004)
281. M. Peter, S.M. Ameer-Beg, M.K.Y. Hughes, M.D. Keppler, S. Prag, M. Marsh, B. Vojnovic, T. Ng, Multiphoton-FLIM quantification of the EGFP-mRFP1 FRET pair for localization of membrane receptor-kinase interactions, Biophys. J. 88, 1224-1237 (2005)
282. Point Source Ltd., Kineflex fibre manipulator, operating instructions
283. T. W. Prow, J. E. Grice, L. L. Lin, R. Faye, M. Butler, W. Becker, E.M.T. Wurm, C. Yoong, T. A. Robertson, H. P. Soyer, M. S. Roberts, Nanoparticles and microparticles for skin drug delivery. Advanced Drug Delivery Reviews 63, 470–491 (2011)
284. P.P. Provenzano, C.T. Rueden, S.M. Trier, L. Yan, S.M. Ponik, D.R. Inman, P.J. Keely, K. W. Eliceiri, Nonlinear optical imaging and spectral-lifetime computational analysis of endogenous and exogenous fluorophores in breast cancer. J. Biomed. Opt. 13(3), 031220-1 to -11 (2008)
285. M. Prummer, B. Sick, A. Renn, U.P. Wild, Multiparameter microscopy and spectroscopy for single-molecule analysis, Anal. Chem. 76, 1633-1640 (2004)
286. X. Qu, J. Wang, Z. Zhang, N. Koop, R. Rahmanzadeh, G. Hüttmann, Imaging of cancer cells by multiphoton microscopy using gold nanoparticles and fluorescent dyes,. J. Biomed. Opt. 13(3) 031217-1 to 7 (2008)
287. E. Ratajczak, A. Pecherski, J. Ramos-Moreno, M. O. Ruonala, FET-assisted determination of CLN3 membrane topology. PLOS ONE 9, e102593 (2014)
288. L. Richert, P. Didier, H. de Rocquigny, Y. Mély, Monitoring HIV-1 Protein Oligomerization by FLIM FRET Microscopy. In: W. Becker (ed.) Advanced time-correlated single photon counting applications. Springer, Berlin, Heidelberg, New York (2015)
289. C. Rickman, C.N. Medine, A. Bergmann, R.R. Duncan, Functionally and spatially distinct modes of MUNC18-syntaxin 1 intercation. JBC 282, 12097-12103 (2007)
290. C. Rickman, C. N. Medine, A. R. Dun, D. J. Moulton, O. Mandula, N. D. Halemani, S. O. Rizzoli, L. H. Chamberlain, and R. R. Duncan, t-SNARE Protein Conformations Patterned by the Lipid Microenvironment. J. Biol. Chem. 285, 13535-13541 (2010)
291. C. Rickman, R. R. Duncan, Munc18/Syntaxin Interaction Kinetics Control Secretory Vesicle Dynamics. J. Biol. Chem. 285, 3965-3972 (2010)
292. I. Riemann, P. Fischer, M. Kaatz, T.W. Fischer, P. Elsner, E. Dimitrov, A. Reif, K. König, Optical tomography of pigmented human skin biopies, Proc. SPIE 5312, 24-34 (2004)

293. R. Rigler, E.S. Elson (eds), Fluorescence Correlation Spectroscopy, Springer Verlag Berlin, Heidelberg, New York (2001)
294. R. Richards-Kortum, R. Drezek, K. Sokolov, I. Pavlova, M. Follen, Survey of endogenous biological fluorophores. In M.-A. Mycek, B.W. Pogue (eds.), Handbook of Biomedical Fluorescence, Marcel Dekker Inc. New York, Basel, 237-264 (2003)
295. A.S. Rinaldi, G. Freund, D. Desplancq, A.P. Sibler, M. Baltzinger, N. Rochel, Y. Mély, P. Didier, E. Weiss, The use of fluorescent intrabodies to detect endogenous gankyrin in living cancer cells. Exp Cell Res. 319(6), 8-49 (2013)
296. B. Riquelme, D. Dumas, J. Valverde, R. Rasia, J.F. Stoltz, Analysis of the 3D structure of agglutinated erythrocyte using CellScan and Confocal microscopy: Characterisation by FLIM-FRET, Proc. SPIE 5139, 190-198 (2003)
297. T. Ritman-Meer, N. I. Cade, D. Richards, Spatial imaging of modifications to fluorescence lifetime and intensity by individual Ag nanoparticles. Appl. Phys. Lett. 91, 123122 (2007)
298. N. Rochel, F. Ciesielski, J. Godet, E. Moman, M. Roessle, C. Peluso-Iltis, M. Moulin, M. Haertlein, P. Callow, Y. Mely, D. I Svergun, D. Moras, Common architecture of nuclear receptor heterodimers on DNA direct repeat elements with different spacings. Nature Structural & Molecular Biology, 18 (5), 564-572 (2011)
299. Roberts, M. S., Dancik, Y., Prow, T.W., Thorling, C.A., Li, L., Grice, J.E., Robertson, T.A., König, K., Becker,W. Non-invasive imaging of skin physiology and percutaneous penetration using 5D (space, time and anisotropy) fluorescence spectral and lifetime imaging with multiphoton and confocal microscopy. European Journal of Pharmaceutics and Biopharmaceutics **77**, 469-488 (2011)
300. A. Rück, F. Dolp, C. Happ, R. Steiner, M. Beil, Time-resolved microspectrofluorometry and fluorescence lifetime imaging using ps pulsed laser diodes in laser scanning microscopes, Proc. SPIE 5139, 166-172 (2003)
301. A. Rück, F. Dolp, C. Hülshoff, C. Hauser, C. Scalfi-Happ, FLIM and SLIM for molecular imaging in PDT, Proc. SPIE 5700 (2005)
302. A. Rück, Ch. Hülshoff, I. Kinzler, W. Becker, R. Steiner, SLIM: A New Method for Molecular Imaging. Micr. Res. Tech. 70, 403-409 (2007)
303. A.L. Rusanov, A.P. Savitsky, Fluorescence resonance energy transfer between fluorescent proteins as powerful toolkits for in vivo studies. Laser Phys. Lett. 8(2) 91-102 (2011)
304. S. Sakadžic, E. Roussakis, M. A. Yaseen, E. T. Mandeville, V. J. Srinivasan1, K. Arai, S. Ruvinskaya, A. Devor, E. H. Lo, S. A. Vinogradov, D. A. Boas, Two-photon high-resolution measurement of partial pressure of oxygen in cerebral vasculature and tissue. Nature Methods 7(9) 755-759
305. M. Salah, N. Samy, M. Fadel, Methylene blue mediated photodynamic therapy for resistant plaque psoriasis. J. Drags Dermatol. 8, 42-49 (2009)
306. W. Y. Sanchez, M. Pastore, I. Haridass, K. König, W. Becker, M. S. Roberts, Fluorescence Lifetime Imaging of the Skin. In: W. Becker (ed.) Advanced time-correlated single photon counting applications. Springer, Berlin, Heidelberg, New York (2015)
307. R. Sanders, A. Draaijer, H.C. Gerritsen, P.M. Houpt, Y.K. Levine, Quantitative pH Imaging in cells using confocal fluorescence lifetime imaging microscopy, Analytical Biochemistry 227, 302-308 (1995)
308. A. Sandqvist, J. K. Björk, M. Åkerfelt, Z. Chitikova, A. Grichine, C. Vourc'h, C. Jolly,§ T. A. Salminen, Y. Nymalm, L. Sistonen, Heterotrimerization of Heat-Shock Factors 1 and 2 Provides a Transcriptional Switch in Response to Distinct Stimuli. Melecular Biology of the Cell 20, 1340-1347 (2009)
309. P. Sarkar, S.V. Koushik, S.S. Vogel, I. Gryczynski, Z. Gryczinski, Photophysical properties of Cerulean and Venus fluorescent proteins. J. Biomed. Opt. 14, 034047-1 to -9 (2009)
310. T. Saxl, F. Khan, D.R. Matthews, Z.-L. Zhi, O. Rolinski, S. Ameer-Beg, J. Pickup, Fluorescence lifetime spectroscopy and imaging of nano-engineered glucose sensor microcapsules based on glucose/galactose-binding protein. Biosensors and Bioelectronics 24, 3229–3234 (2009)
311. R. H. Schirmer, B. Coulibaly, A. Stich, M. Scheiwein, H. Merkle, J. Eubel, K. Becker, H. Becher, O. Müller, T. Zich, W. Schiek, B. Kouyate, Methylene blue as an antimalarial agent. Redox Report 8, 272-275 (2003)
312. A. C. Schüller, Z. Ahmed, J. A. Levitt , K. M. Suen, K. Suhling and J. E. Ladbury, Indirect recruitment of the signalling adaptor Shc to the fibroblast growth factor receptor 2 (FGFR2). Biochem. J. 416, 189–199 (2008)
313. D. Schweitzer, M. Hammer, F. Schweitzer, R. Anders, T. Doebbecke, S. Schenke, E. R. Gaillard, In vivo measurement of time-resolved autofluorescence at the human fundus, J. Biomed. Opt. **9**, 1214-1222 (2004)
314. D. Schweitzer, S. Schenke, M. Hammer, F. Schweitzer, S. Jentsch, E. Birckner, W. Becker, Towards Metabolic Mapping of the Human Retina. Micr. Res. Tech. 70, 403-409 (2007)

315. D. Schweitzer, Quantifying fundus autofluorescence. In: N. Lois, J.V. Forrester, eds., Fundus autofluorescence. Wolters Kluwer, Lippincott Willams & Wilkins (2009)
316. D. Schweitzer, Metabolic Mapping. In: F.G. Holz, R.F. Spaide (eds), Medical retina, Essential in Opthalmology, Springer (2010)
317. D. Schweitzer, E.R. Gaillard, J. Dillon, R.F. Mullins, S. Russell, B. Hoffmann, S. Peters, M. Hammer, C. Biskup, Time-Resolved Autofluorescence Imaging of Human Donor Retina Tissue from Donors with Significant Extramacular Drusen. IOVS, 53, 3376-3386 (2012)
318. S. Sever, J. Skoch, S. Newmyer, R. Ramachandran, D. Ko, M. McKee, R. Bouley, D. Ausiello, B. T Hyman, B. J. Bacskai, Physical and functional connection between auxilin and dynamin during endocytosis. EMBO J. 25, 4163-4174 (2006)
319. S. Sever, J. Skoch, B. J. Bacskai, S. Newmyer, Assays and functional properties of auxilin-dynamin interactions. Methods Enzymol. 404, 570-585 (2005)
320. A.L. Serrano, O. Bilsel, F. Gai, Native State Conformational Heterogeneity of HP35 Revealed by Time-Resolved FRET. J Phys Chem B. 116(35):10631-8 (2012)
321. Q.-H. Shen, Y, Saijo, S. Mauch, C. Biskup, S. Bieri, B. Keller, H. Seki, B. Ülker, I.E. Somssich, P. Schulze-Leftert, Nuclear activity of MLA immune response links isolate-specific and basal resistance responses. Science Express, www.scienceexpress.org / 21 December 2006 / Page 1 / 10.1126/science.1136372
322. M. Shibata, S. Ichioka, J. Ando, A. Kamiya, Microvascular and interstitial PO2 measurement in rat skeletal muscle by phosphorescence quenching. J. Appl. Physiol. 91, 321-327 (2001)
323. M. C. Skala, K. M. Riching, D. K. Bird, A. Dendron-Fitzpatrick, J. Eickhoff, K. W. Eliceiri, P. J. Keely, N. Ramanujam, In vivo multiphoton fluorescence lifetime imaging of protein-bound and free nicotinamide adenine dinucleotide in normal and precancerous epithelia. J. Biomed. Opt. 12 02401-1 to 10 (2007)
324. M. C. Skala, K. M. Riching, A. Gendron-Fitzpatrick, J. Eickhoff, K. W. Eliceiri, J. G. White, N. Ramanujam, In vivo multiphoton microscopy of NADH and FAD redox states, fluorescence lifetimes, and cellular morphology in precancerous epithelia, PNAS 104, 19494-19499 (2007)
325. A. M. Smyth, C. Rickman, R. R. Duncan, Vesicle Fusion Probability Is Determined by the Specific Interactions of Munc18. J. Biol. Chem. 285, 38141-38148 (2010)
326. M. Snippe, J.W. Borst, R. Goldbach, R. Kormelik, The use of fluorescence microscopy to visualise homotypic interactions of tomato spotted wilt virus nucleocapsid protein in living cells, J. Vir. Meth. 125, 12-15 (2005)
327. P.T.C. So, K.H. Kim, L. Hsu, P. Kaplan, T. Hacewicz, C.Y. Dong, U. Greuter, N. Schlumpf, C. Buehler, Two-photon microscopy of tissues, in M.-A. Mycek, B.W. Pogue (eds.), Handbook of Biomedical Fluorescence, Marcel Dekker, New York, Basel, 181-208 (2003)
328. P.V. Solntsev, K.L.Spurgim, J.R. Sabin, A.A. Heikal, V.N.Nemykin, Photoinduced charge transfer in short-distance ferrocenylsubphtahlocyanine dyads. Inorg. Chem. 51, 6537-6547 (2012)
329. L. Song, C.A.G.O. Varma, J.W. Verhoeven, H.J. Tanke, Influence of the triplet excited state on the photobleaching kinetics of fluoresceien in microscopy. Biophys. J. 70, 2959-2968 (1996)
330. M. Stagi, P. Gorlovoy, S. Larionov, K. Takahashi, H. Neumann, Unloading kinesin transported cargoes from the tubulin track via the inflammatory c-Jun N-terminal kinase pathway. The FASEB Journal 20, E1-E12 (2006)
331. M. H. Stewart, A. L. Huston, A. M. Scott, A. L. Efros, J. S. Melinger, K. Boeneman Gemmill, S. A. Trammell, J. B. Blanco-Canosa, P E. Dawson, I. L. Medintz, Complex Förster energy transfer interactions between semiconductor quantum dots and a redox-active osmium assembly. ACS Nano 6, 5330-5347 (2012)
332. S. J. Strickler, R. A. Berg, Relationship between absorption intensity and fluorescence lifetime of molecules, J. Chem. Phys. 37, 814–822 (1962)
333. C. Strohhöfer, T. Förster, D. Chorvat, P. Kasak, I. Lacik, M. Koukaki, S. Karamanou A.s Economoude, Quantitative analysis of energy transfer between fluorescent proteins in CFP–GBP–YFP and its response to Ca^{2+}. Phys. Chem. Chem. Phys. 13 17852-17863 (2011)
334. C.D. Stubbs, S.W. Botchway, S.J. Slater, A.W. Parker, The use of time-resolved fluorescence imaging in the study of protein kinase C localisation in cells. BioMed Central 6:22 (2005), available on www.biomedcentral.com/1471-2121/6/22
335. H. Studier, W. Becker, Megapixel FLIM. Proc. SPIE 8948 (2014)
336. K. Suhling, D.M. Davis, Z. Petrasek, J. Siegel, D. Phillips, The influence of the refractive index on EGFP fluorescence lifetimes in mixtures of water and glycerol, Proc. SPIE **4259**, 91-101 (2001)
337. K. Suhling, J. Siegel, D. Phillips, P.M.W. French, S. Lévêque-Fort, S.E.D. Webb, D.M. Davis, Imaging the environment of green fluorescent protein, Biophysical J. **83**, 3589-3595 (2002)
338. K. Suhling, L. M. Hirvonen, J. A. Levitt, P.-H. Chung, C. Tregido, A. le Marois, D. Rusakov, K. Zheng, Fluorescence Lifetime Imaging (FLIM): Basic Concepts and Recent Applications. In: W. Becker (ed.)

Advanced time-correlated single photon counting applications. Springer, Berlin, Heidelberg, New York (2015)
339. Y. Sun, C.F. Booker, S. Mumari, R.N. Day, M. Davidson, A. Periasamy, Characterisation of an orange acceptor fluorescent protein for sensitzed spectral fluorescence resonance energy transfer microscopy using a white light laser. J. Biomed. Opt. 14(5) 054009-1 to 11 (2009)
340. Y. Sun, A. Periasamy, Additional correction for energy transfer efficiency calculation in filter-based Förster resonance energy transfer for a more accurate result. J. Biomed. Opt. 15(2), 020513 (2010).
341. Y. Sun, C. Rombola, V. Jyothikumar, A. Periasamy, Förster resonance energy transfer microscopy and spectroscopy to localize protein-protein interactions in live cells. Cytometry A, 83A(9), 780-793 (2013)
342. T. Tabouillot, H.S. Muddana, P.J. Butler, Endothelial membrane sensitivity to shear stress is lipid domain dependent. Cell. Mol. Bioeng. 4(2), 169-181 (2011)
343. I. Texier, M. Goutayer, A. Da Silva, L. Guyon, N. Djaker, V. Josserand, E. Neumann, J. Bibette, F. Vinet, Cyanine-loaded lipid nanoparticles for improved in vivo fluorescence imaging. J. Biomed. Opt. 14(5), 054005-1 to 11 (2009)
344. C. Thaler, S.V. Koushik, H.L. Puhl, P.S. Blank, S.S. Vogel, Structural rearrangement of CaMKIIα catalytic domains encodes activation. PNAS 0901913106 (2009)
345. P. Theer, M.T. Hasan, W. Denk, Multi-photon imaging using a Ti:sapphire regenerative amplifier, Proc. SPIE 5139, 1-6 (2003)
346. Z. Timsah, Z. Ahmed, C.-C. Lin, F. A. Melo, L. J. Stagg, P. G. Leonard, P. Jeyabal, J. Berrout, R. G. O'Neil, M. Bogdanov, J. E. Ladbury, Competition between Grb2 and Plcγ1 for FGFR2 regulates basal phospholipase activity and invasion. Nature Structural & Molecular Biology 21, 180-188 (2014)
347. C. Toncelli, O. V. Arzhakova, A. Dolgova, A. L. Volynskii, N. F. Bakeev, J. P. Kerry, D. B. Papkovsky, Oxygen-sensitive phosphorescent nanomaterials produced from high density polyethylene films by local solvent-crazing. Anal. Chem. 86(3), 1917-23 (2014)
348. B. Treanor, P.M.P. Lanigan, K. Suhling, T. Schreiber, I. Munro, M.A.A. Neil, D. Phillips, D.M. Davis, P.M.W. French, Imaging fluorescence lifetime heterogeneity applied to GFP-tagged MHC protein at an immunological synapse, J. Microsc. 217, 36-43 (2005)
349. C. Tregido, J.A. Levitt, K. Suhling, Effect of refractive index on the fluorescence lifetime of green fluorescent protein. J. Biomed. Opt. 13(3), 031218-1 to -8 (2008)
350. C. J. Tynan, S. K. Roberts, D. J. Rolfe, D. T. Clarke, H. H. Loeffler, J. Kästner, M. D. Winn, P. J. Parker, M. L. Martin-Fernandez, Human Epidermal Growth Factor Receptor (EGFR) Aligned on the Plasma Membrane Adopts Key Features of Drosophila EGFR Asymmetry. Mol. Cell. Biol 31(11) 2241-2252 (2011)
351. Y. Ueda, S. Kwok, Y. Hayashi, Application of FRET probes in the analysis of neuronal plasticity, Frontiers in neural circuits 7, 163 (2013)
352. Y. Ueda, Y. Hayashi, PIP_3 regulates spinule formation in dentritic spines structural long-term potentiation. J. Neurosci. 33(27) 11040-11047 (2013)
353. K. Uemura, C. M. Lill, M. Banks, M. Asada, N. Aoyagi, K. Ando, M. Kubota, T. Kihara, T. Nishimoto, H. Sugimoto, R. Talahashi, B. T. Hyman, S. Shimohama, O. Berezovska, A. Kinoshita, N-cadherin-based adhesion anhances Aβ releases and decreases $Aβ_{42/40}$ ratio. J. Neurochem. 108, 350-360 (2009)
354. M. Valkonen, E. R. Kalkman, M. Saloheimo, M. Penttilä, N. D. Read, R. R. Duncan, Spatially segregated snare protein interactions in living fungal cells. JBC 282, 22775-22785 (2007)
355. M.A.M.J. Van Zandvoort, C.J. de Grauw, H.C. Gerritsen, J.L.V. Broers, M.G.A. Egbrink, F.C.S. Ramaekers, D.W. Slaaf, Discrimination of DNA and RNA in cells by a vital fluorescent probe: Lifetime imaging of SYTO13 in healthy and apoptotic cells, Cytometry **47**, 226-232 (2002)
356. H.D. Vishwasrao, A. A. Heikal, K.A. Kasischke, W. W. Webb, Conformational Dependence of Intracellular NADH on Metabolic State Revealed by Associated Fluorescence Anisotropy. J. Biol. Chem. 280, 25119-25126 (2005)
357. T. Vo-Dinh, Biomedical Photonics Handbook, CRC Press (2003)
358. S. S. Vogel, C. Thaler, S. V. Koushik, Fanciful FRET. Sci. STKE 2006, re2 (2006)
359. S.S. Vogel, C. Thaler, P.S. Blonk, S.V. Koushik, Time-Resolved Fluorescence Anisotropy. In: A. Periasamy, R.M. Clegg, FLIM microscopy in Biology and medicine. Taylor & Francis (2009)
360. C.A. von Arnim, A. Kinoshita, I.D. Peltan, M.M. Tangredi, L. Herl, B.M. Lee ,R. Spoelgen, T.T. Hshieh, S. Ranganathan, F.D. Battey, C.X. Liu, B.J. Bacskai, S. Sever,M.C. Irizarry, D.K. Strickland, B.T. Hyman, The low density lipoprotein receptor-related protein (LRP) is a novel beta-secretase (BACE1) substrate. J Biol Chem. 280, 7777-7785 (2005)
361. H. Wabnitz, M. Mazurenka, L. Di Sieno, G. Boso, W. Becker, K. Fuchs, D. Contini, A. Dalla Mora, A. Tosi, R. Macdonald, A. Pifferi, Time-domain diffuse optical imaging of tissue by non-contact scanning. In: W. Becker (ed.) Advanced time-correlated single photon counting applications. Springer, Berlin, Heidelberg, New York (2015)

362. P. Walczysko, U. Kuhlicke, S. Knappe, C. Cordes, T.R. Neu, In Situ Activity of Suspended and Immobilized Microbial Communities as Measured by Fluorescence Lifetime Imaging. Appl. Environ. Mocrobiol. 74, 294-299 (2008)
363. J.G. White, W.B. Amos, M. Fordham, An evaluation of confocal versus conventional imaging of biological structures by fluorescence light microscopy, J. Cell Biol. 105, 41-48 (1987)
364. J. Widengren, V. Kudryavtsev, M. Antonik, S. Berger. M. Gerken, C. A. M. Seidel, Single-molecule detection and identification of multiple species by multiparameter fluorescence detection. Anal.Chem. 78, 2039-2050 (2006)
365. C. D. Wilms, H. Schmidt, and J. Eilers, Quantitative two-photon Ca^{2+} imaging via fluorescence lifetime analysis, Cell Calcium 40, 73-79 (2006)
366. T. Wilson, C. Sheppard, Theory and practice of scanning optical microscopy. Academic Press (1984)
367. G. T. Wondrak, NQQO1-activated phenothiazinium redoc cyclers for the targeted bioreductive induction of cancer cell apaptosis. Free Radic. Biol. Med. 15, 178-190 (2007)
368. Y. Wu, Y. Qu, Combined depth- and time-resolved autofluorescence spectroscopy of epithelial tissue. Opt. Lett. 31, 1833-1835 (2006)
369. C. Xu, W.W. Webb, Measurement of two-photon excitation cross sections of molecular fluorophores with data from 690 to 1050 nm. J. Opt. Soc. Am. B 13, 481-491 (1996)
370. R. Yasuda, C.D. Harvey, H. Zhong, A. Sobczyk, L. van Aelst, K. Svoboda, Supersensitive Ras activation in dendrites and spines revealed by two-photon fluorescence lifetime images. Nature Neuroscience 9 (2), 238-291 (2006)
371. J. Yguerabide, Nanosecond fluorescence spectroscopy of macromolecules, Meth. Enzymol. 26, 498-578 (1972)
372. I. Yudushkin, R.D.Vale, Imaging T-cell receptor activation reveals accumulation of tyrosine-phosphorylated CD3ζ in the endosomal compartment. PNAS 107, 22128-22133 (2010)
373. Y.-L. Zhang, J. A. Frangos, M.S Chachisvilis, Mechanical stimulus alters conformation of type 1 parathyroid hormone receptor in bone cells. Am. J. Physiol. Cell Physiol. 296, C1391-C1399 (2009)
374. Y.-L. Zhang, H. Tavakoli, M. Chachisvilis, Apparent PKA activity responds to intermittent hypoxia in bone cells: A redox pathway? Am. J. Physiol. Heart Circ. Physiol. 299, H225–H235 (2010)
375. X. Zhang, S. Shastry, S.E. Bradforth , J.L.Nadeau, Nuclear uptake of ultrasmall gold-doxorubicin conjugates imaged by fluorescence lifetime imaging microscopy (FLIM) and electron microscopy. Nanoscale 7(1), 240-251 (2014)